




Electrokinetic and dielectric response of a concentrated salt-free colloid: Different approaches to counterion finite-size effects

F. Carrique ^{*}*Departamento de Física Aplicada I Facultad de Ciencias, Universidad de Málaga, 29071 Málaga, Spain*E. Ruiz-Reina [†]*Departamento de Física Aplicada II Escuela de Ingenierías Industriales Universidad de Málaga, 29071 Málaga, Spain*F. J. Arroyo [‡]*Departamento de Física Facultad de Ciencias Experimentales, Universidad de Jaén, 23071 Jaén, Spain*M. L. Jiménez,[§] S. Ahualli,^{||} and A. V. Delgado [¶]*Departamento de Física Aplicada Facultad de Ciencias, Universidad de Granada, 18071 Granada, Spain*

(Received 22 December 2021; accepted 25 February 2022; published 13 June 2022)

In the present work, a general model is developed for the electrokinetics and dielectric response of a concentrated salt-free colloid that takes into account the finite size of the counterions released by the particles to the solution. The effects associated with the counterion finite size have been addressed using a hard-sphere model approach elaborated by Carnahan and Starling [N. F. Carnahan and K. E. Starling, Equation of state for nonattracting rigid spheres, *J. Chem. Phys.* **51**, 635 (1969)]. A more simple description of the finite size of the counterions based on that by Bikerman has also been considered for comparison. The studies carried out in this work include predictions on the effect of the finite counterion size on the equilibrium properties of the colloid and its electrokinetic and dielectric response when it is subjected to constant or alternating electric fields. The results show how important the counterion finite-size effects are for most of the electrokinetic and dielectric properties of highly charged and concentrated colloids, mainly for the static and dynamic electrophoretic mobilities. Furthermore, new insights are provided on the counterion condensation effect when counterions are allowed to have finite size. Focus is placed on the changes undergone by their concentration in the condensation layer for low-salt and highly charged colloids.

DOI: [10.1103/PhysRevE.105.064604](https://doi.org/10.1103/PhysRevE.105.064604)

I. INTRODUCTION

Strictly, a pure or ideal salt-free colloid is composed of a system of charged particles dispersed in a solution where the only ions present stem typically from the dissociation of particle surface chemical groups. Such ions are usually called released counterions. This countercharge in solution plus the charged particles form an electrically neutral system. Of course, colloids in aqueous solutions under supposedly salt-free conditions (no external salt added to the system) deviate from the concept of an ideal salt-free colloid because of the presence of hydronium and hydroxyl ions from water dissociation, and possibly others from carbon dioxide contamination, if the colloid is open to the atmosphere. A colloid in such conditions is usually called a “realistic” salt-free one.

This is the situation addressed in a recent paper [1], where a new ac electrokinetic model for concentrated salt-free spherical colloids with arbitrary conditions for particles and aqueous solution was presented. This theory incorporates a realistic chemistry for the solution in order to improve the comparison with the experiments in aqueous media. Thus, a realistic nonequilibrium scenario standing for association-dissociation processes in the chemical reactions was used, with special emphasis on incorporating the effect of the finite size of all ionic and neutral species on the theoretical electrokinetic response. The results showed that the consideration of finite ion-size effects, mainly at high frequencies of the electric field and for highly charged colloids, becomes crucial to give us a more complete description of the electrokinetic response of the colloid. Such analysis was carried out by using Bikerman-like (Bk) equilibrium activity coefficients [2,3] for all ionic and neutral species (water molecules excluded) instead of more exact descriptions like for example that by Carnahan and Starling [4] (C-S). The reason for using Bikerman’s instead of C-S’s approach was the huge mathematical difficulties involved in the calculation of all frequency dependencies in the case of concentrated realistic salt-free colloids out of equilibrium with the C-S formalism.

^{*} carrique@uma.es[†] eruizr@uma.es[‡] fjarroyo@ujaen.es[§] jimenez@ugr.es^{||} sahualli@ugr.es[¶] adelgado@ugr.es

On the other hand, an increasing interest is nowadays being dedicated to the study of salt-free colloids from both theoretical and experimental points of view [5–9]. The salt-free colloids can form ordered phases with phase transitions at low particle concentrations with a clear resemblance with molecular or atomic crystals [10–12]. That is the reason why they are usually called colloidal crystals or glasses. In salt-free conditions the long-range repulsive electrical forces are responsible to a large extent of the formation of such crystals at moderately low particle concentrations, as the screening effect on particle charge of the ionic species in solution is quite low in comparison with the conditions found in colloids in electrolyte solutions.

In addition, a process of counterion condensation takes place close to the particle surface, beyond a critical charge density [5,7,8,13–16]: For highly charged salt-free colloids, a layer of counterions condenses onto the particle surface because of a competition between a favorable gain in electrostatic energy as counterions get closer to the particle surface and an unfavorable loss of entropy as counterions move toward the surface instead of moving to farther regions less populated by counterions in the solution. This phenomenon plays a very important role in general electrostatic soft matter, not only controlling the stability of colloids but also the self-assembly of different (bio)molecules [17,18]. The counterion condensation leads to the concept of effective or renormalized particle charge as the condensation layer partly neutralizes the bare structural particle charge [16,19]. Hence, the enormous interest of theoreticians in understanding the phenomenon of the counterion condensation that only takes place in the limit of salt-free or very low salt conditions. Also, there is an increasing effort dedicated to perform simulations and to develop theoretical studies with charged nonpolar colloids as model systems for the prediction of the equilibrium and nonequilibrium dynamics of counterions, as nonpolar colloids allow the design of experiments in electrostatic regimes that are inaccessible to typical colloids in electrolyte solutions [8,20,21]. But there are also a large number of experimental phenomena where the salt-free colloids are gaining relevance, particularly in biomedical applications. It has been referred for example that the electrohydrodynamic separation of DNA from BSA is highly improved in salt-free environments [22]. Also, that the salt-free extraction of some biosurfactants may avoid phytotoxic conditions [23], or that a better determination of the protein content and biomass of stabilized bacterial cells can be obtained in salt-free environments [24], as well as improvements in the dyeing of cotton that can be achieved if it is made in salt-free media [25,26], etc.

In the last few years and due to its importance, different authors have explored the use of more elaborate models (like the above-mentioned C-S approach [4]) to manage the finite ionic size effects in the study of the electrokinetics of dilute colloids in electrolyte solutions [27–30]. Quite recent studies concerning the equilibrium of concentrated salt-free colloids (no external electric field applied) and an analytical approximation for the electrophoretic mobility of a spherical particle in constant electric fields in such systems were addressed by Ohshima according to the C-S model [7].

In the present work we face the problem of the finite size of the released counterions and its effect on the equilibrium

properties and electrokinetic and dielectric responses under constant or alternating electric fields of an ideal concentrated salt-free colloid according to the mentioned C-S approach, which is physically more consistent than others [31], and mainly for a couple of reasons. First, solving the mathematical problems for an ideal salt-free case with the C-S approach might help to address the realistic one. Second, up to date there is no general model for the electrokinetics of an ideal and concentrated salt-free colloid with the C-S approach, unlike the case of dilute colloids in electrolyte solutions where continuous advances even beyond the C-S approach are being published [3]. But a realistic concentrated salt-free colloid has two singular characteristics that differentiate it from the dilute case when the C-S approach is concerned. One is linked to the coupling between the released countercharge and the particle charge in salt-free colloids, as the electrical neutrality in the system has to be fulfilled. However, the simultaneous consideration of both ionic couplings [1] and finite ion size effects according to the C-S formalism, would lead to almost unaffordable mathematical problems in the numerical resolution of the electrokinetic equations. The other characteristic refers to the higher complexity of the concentrated case, either ideal or realistic, in comparison with the dilute one, as it is necessary to manage the electrohydrodynamic particle-particle interactions as particle concentration increases, at least in an average way. In the concentrated regime there is no clear information about bulk properties (*a priori* known for the dilute problem) and we can even ask whether the definition of a bulk property makes sense or not in highly concentrated colloids due to the close presence of neighbor particles around a given one.

In summary, in the present work and as a first approach, a complete electrokinetic model valid for ideal and concentrated salt-free colloids under the presence of constant (dc) or alternating (ac) electric fields will be developed. Particular attention will be paid to the role that the finite size of the released counterions plays on electrokinetic and dielectric properties as the dc or ac electrophoretic mobilities, dc and ac conductivities and relative permittivity of the colloid. Two parallel studies will be performed to achieve this goal according, respectively, to Bikerman's-related [2] and Carnahan-Starling [4] models, and a global comparison between their predictions will be made. Previously, the equilibrium case will be analyzed in terms of the local electric potential and the local concentration of counterions around a given particle. In order to manage the particle-particle electrohydrodynamic interactions in the concentrated regime, a cell model will be used [32,33].

II. FINITE-SIZE EFFECTS AT EQUILIBRIUM

In this section we will explore the effect at equilibrium of the excluded volume of ions in an ideal salt-free colloid. To that aim, use will be made of the Carnahan-Starling activity coefficient, γ_{CS}^0 , of the counterions released from the particles to the solution [4] before addressing the study of the electrokinetic response of our system in the presence of constant or alternating electric fields. A comparison with a Bikerman-like activity coefficient γ_{Bk}^0 depending on the packing fraction of counterions [2,3] will also be made. As it was done in previous

studies, a spherical cell model will be used to account, in an average sense, for the particle-particle electrohydrodynamic interactions in the colloid [32]. According to this model, the outer radius of the cell b , will be chosen by equating the particle volume fraction ϕ of the whole colloid with that obtained within a single cell. Hence, this will be composed of one particle of radius a at its center and a surrounding region of solution of radius b such that $\phi = (a/b)^3$.

We assume for the moment that the system consists of a collection of spherical nanoparticles, with radius a , and surface charge density σ in a solution with relative permittivity ϵ_{rs} and viscosity η_s . The activity coefficient γ_{CS}^0 of the only ionic species present in the solution, that is, the released counterions that counterbalance the particles charge, is given according to Carnahan-Starling by [3,4]:

$$\gamma_{CS}^0(r) = \exp\left(\frac{\varphi^0(r)\{8 - 9\varphi^0(r) + 3[\varphi^0(r)]^2\}}{[1 - \varphi^0(r)]^3}\right), \quad (1)$$

where $\varphi^0(r)$ is the counterion volume fraction at a radial distance r from the center of the particle, and it can be related to the counterion concentration $n^0(r)$ as:

$$\varphi^0(r) = n^0(r)V_c = n^0(r)\frac{4}{3}\pi R^3, \quad (2)$$

where V_c is the volume of a spherical counterion of radius R .

On the other hand, the activity coefficient γ_{Bk}^0 of the counterions according to a modification of the original Bikerman expression, may be given by [34]:

$$\gamma_{Bk}^0(r) = \frac{1}{1 - \left[\frac{\varphi^0(r)}{p}\right]} = \frac{1}{1 - \left[\frac{n^0(r)}{n^{\max}}\right]} = \frac{1}{1 - \left[\frac{n^0(r)V_c}{p}\right]}, \quad (3)$$

where p is the packing factor, and n^{\max} is a maximum counterion concentration that is defined by:

$$n^{\max} = \frac{1}{V_e} \quad (4)$$

as the inverse of the effective volume V_e occupied per counterion in a unit crystal cell for a given packing. Also it is fulfilled that:

$$p = \frac{V_c}{V_e} \quad (5)$$

and the counterion volume fraction $\varphi^0(r)$ may then be expressed by:

$$\varphi^0(r) = p \left[\frac{n^0(r)}{n^{\max}} \right]. \quad (6)$$

For instance, for face-centered cubic packing: $p_{fcc} = \pi\sqrt{2}/6 = 0.74$ and $V_{ecc} = 4R^3\sqrt{2}$; for simple cubic packing: $p_{sc} = \pi/6 = 0.524$ and $V_{esc} = (2R)^3$; for body-centered cubic packing: $p_{bcc} = \pi\sqrt{3}/8 = 0.68$ and $V_{ebc} = 32\sqrt{3}R^3/9$; and for random close packing: $p_{rp} = 0.64$ and $V_{erp} = (4\pi R^3)/(3p_{rp})$.

In Fig. 1 is displayed the natural logarithm of C-S and Bk (for $p = 0.74$) activity coefficients as a function of the counterion volume fraction φ^0 . Note that the C-S activity coefficient departs from unity much faster than the Bk one as we increase the concentration of counterions. In other words, the population of ions is lowered (with respect to the usual pointlike approximation) by C-S calculations to a larger extent

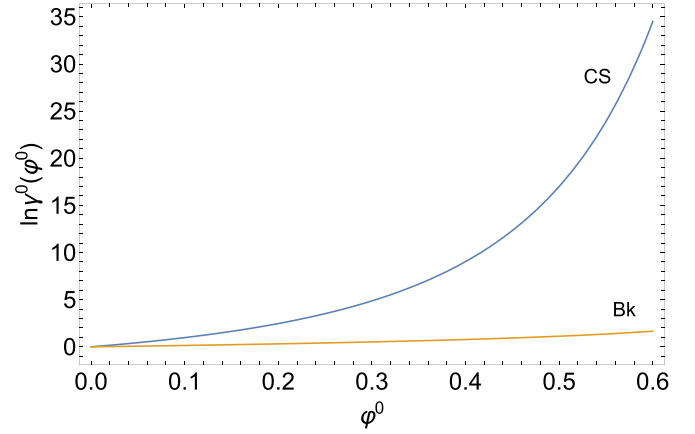


FIG. 1. Natural logarithm of the counterion activity coefficient γ^0 as a function of the counterion volume fraction φ^0 according to Bikerman [Bk; see Eq. (3)] for $p = 0.74$ and Carnahan-Starling [C-S; Eq. (1)]

than Bk does, at least where the concentration is large, i.e., close to highly charged interfaces. Unless otherwise specified, in the following $\gamma^0(r)$ will stand for both possible activity coefficients, C-S or Bk.

The equilibrium electrochemical potential for the counterions can be expressed as:

$$\mu^0(r) = \mu^\infty + ze\Psi^0(r) + k_B T \ln[\gamma^0(r) n^0(r)], \quad (7)$$

where μ^∞ and z are the electrochemical potential of the counterions at a standard state and their valence, $\Psi^0(r)$ is the equilibrium electric potential at a radial distance r from the center of the particle, e is the elementary electric charge, k_B is the Boltzmann constant, and T is the absolute temperature.

In the absence of an external electric field, the Nernst-Planck equation can be solved for the equilibrium concentration of counterions in terms of the equilibrium electric potential, as the gradient of its electrochemical potential must be zero in such conditions:

$$\nabla\mu^0(r) = \nabla\{\mu^\infty + ze\Psi^0(r) + k_B T \ln[\gamma^0(r) n^0(r)]\} = 0. \quad (8)$$

Accordingly, at an arbitrary radial distance r and at the outer radius $r = b$ of the cell where the equilibrium electric potential $\Psi^0(b)$ is set to zero, the electrochemical potential must fulfill the equality:

$$\gamma^0(r) n^0(r) = \gamma^0(b) n^0(b) e^{-\frac{ze}{k_B T} \Psi^0(r)} \quad (9)$$

and the modified Poisson-Boltzmann equation (MPB) accounting for the finite size of the counterions is then (see the equivalent procedure by Ohshima in Ref. [7]):

$$\begin{aligned} \nabla^2\Psi^0(r) &= \frac{d^2\Psi^0(r)}{dr^2} + \frac{2}{r} \frac{d\Psi^0(r)}{dr} = -\frac{ze}{\epsilon_0\epsilon_{rs}} n^0(r) \\ &= -\frac{ze}{\epsilon_0\epsilon_{rs}} \frac{\gamma^0(b) n^0(b)}{\gamma^0(r)} e^{-\frac{ze}{k_B T} \Psi^0(r)}, \end{aligned} \quad (10)$$

where ϵ_0 is the electric permittivity of a vacuum.

For the Bikerman case one can write [1]:

$$\left[\frac{\gamma^0(b)}{\gamma^0(r)} \right] = \frac{1}{1 + \frac{n^0(b)}{n^{\max}} \left[e^{-\frac{ze}{k_B T} \Psi^0(r)} - 1 \right]} \quad (11)$$

and then

$$n^0(r) = \frac{n^0(b) e^{-\frac{ze}{k_B T} \Psi^0(r)}}{1 + \frac{n^0(b)}{n^{\max}} \left[e^{-\frac{ze}{k_B T} \Psi^0(r)} - 1 \right]} \quad (12)$$

so the MPB Eq. (10) can also be expressed by:

$$\frac{d^2 \Psi^0(r)}{dr^2} + \frac{2}{r} \frac{d\Psi^0(r)}{dr} = -\frac{ez}{\varepsilon_0 \varepsilon_{rs}} \frac{n^0(b) e^{-\frac{ze}{k_B T} \Psi^0(r)}}{1 + \frac{n^0(b)}{n^{\max}} \left[e^{-\frac{ze}{k_B T} \Psi^0(r)} - 1 \right]}. \quad (13)$$

No closed expression in terms of the equilibrium electric potential as that in Eq. (13) is attainable for the Carnahan-Starling approach, due to the complex dependence on counterion volume fraction of the C-S activity coefficient [see Eq. (1)]. Whatever the case, global charge neutrality in the cell is obeyed, so that

$$\begin{aligned} 4\pi a^2 \sigma &= -ez \int_a^b n^0(r) 4\pi r^2 dr \\ &= -4\pi ez \gamma^0(b) n^0(b) \int_a^b \frac{e^{-\frac{ze}{k_B T} \Psi^0(r)}}{\gamma^0(r)} r^2 dr \end{aligned} \quad (14)$$

is fulfilled. For the Bikerman case, the latter equation can also be expressed as:

$$4\pi a^2 \sigma = -\frac{4\pi ez}{a^2} \int_a^b \frac{n^0(b) e^{-\frac{ze}{k_B T} \Psi^0(r)}}{1 + \frac{n^0(b)}{n^{\max}} \left[e^{-\frac{ze}{k_B T} \Psi^0(r)} - 1 \right]} r^2 dr. \quad (15)$$

The necessary boundary conditions to numerically solve the general MPB equation [see Eq. (10)] for the equilibrium electric potential, or that specific for the Bikerman approach in Eq. (13) are

$$\frac{d\Psi^0}{dr}(b) = 0, \quad \frac{d\Psi^0}{dr}(a) = -\frac{\sigma}{\varepsilon_{rs} \varepsilon_0}, \quad (16)$$

that can be obtained by applying Gauss theorem to the inner $r = a$ and outer $r = b$ surfaces of the cell, also imposing its electroneutrality.

In the recent past, a numerical procedure based on the generation of an equivalent third-order differential MPB equation for the equilibrium electric potential, that explicitly eliminates the unknown counterion concentration at the outer surface of the cell $n^0(b)$, has been reported [35]. This procedure avoids tedious iterations of the typical numerical resolutions of this kind of equations. We previously need to express the equilibrium counterion concentration and its first radial derivative in terms of increasing order derivatives of the equilibrium electric potential. Also, an extra boundary condition is explicitly needed to solve the third-order MPB equation, and our choice is that related to the origin for the equilibrium electric potential, which is set at the outer surface of the cell:

$$\Psi^0(b) = 0. \quad (17)$$

The third-order differential equation procedure allows us to obtain the following MPB equation (see the Appendix for details):

$$\begin{aligned} \frac{d^3 \Psi^0(r)}{dr^3} + \frac{2}{r} \frac{d^2 \Psi^0(r)}{dr^2} - \frac{2}{r^2} \frac{d\Psi^0(r)}{dr} \\ = -\frac{ze}{k_B T} \left[\frac{d^2 \Psi^0(r)}{dr^2} + \frac{2}{r} \frac{d\Psi^0(r)}{dr} \right] \frac{d\Psi^0(r)}{dr} \Lambda(r) \end{aligned} \quad (18)$$

with the $\Lambda(r)$ function for the C-S and Bk approaches being defined by:

$$\Lambda(r)_{CS} = \frac{1 - 4\varphi^0(r) + 6\varphi^0(r)^2 - 4\varphi^0(r)^3 + \varphi^0(r)^4}{1 + 4\varphi^0(r) + 4\varphi^0(r)^2 - 4\varphi^0(r)^3 + \varphi^0(r)^4} \quad (19)$$

$$\Lambda(r)_{Bk} = 1 - \left[\frac{\varphi^0(r)}{p} \right] \quad (20)$$

and the counterion volume fraction in Eqs. (19) and (20) by:

$$\varphi^0(r) = -\frac{\varepsilon_0 \varepsilon_{rs} V_c}{ze} \left[\frac{d^2 \Psi^0(r)}{dr^2} + \frac{2}{r} \frac{d\Psi^0(r)}{dr} \right] \quad (21)$$

according to Eqs. (2) and (10). The pointlike case is attained by making $\varphi^0(r) \rightarrow 0$ in Eqs. (19) and (20), which yields $\Lambda(r) \rightarrow 1$. In that limit Eq. (18) becomes the third-order MPB equation for an ideal salt-free colloid with pointlike counterions that was already derived in a previous paper [36].

Once the equilibrium electrical potential is obtained, the equilibrium counterion concentration can be derived from Poisson equation [see the left side of Eq. (10)] as:

$$n^0(r) = -\frac{\varepsilon_0 \varepsilon_{rs}}{ze} \left[\frac{d^2 \Psi^0(r)}{dr^2} + \frac{2}{r} \frac{d\Psi^0(r)}{dr} \right]. \quad (22)$$

The predictions concerning equilibrium electrical potential and counterion concentration will be analyzed in the next section.

III. SOME NUMERICAL RESULTS FOR THE EQUILIBRIUM ELECTRIC POTENTIAL AND COUNTERION CONCENTRATION

We explore below in Fig. 2 some numerical results of the effect of the counterion size on both (a) the dimensionless equilibrium electric potential $\Psi_{\text{dim}}^0 = e\Psi^0/(k_B T)$ and (b) the molar equilibrium counterion concentration $c^0 = n^0/(10^3 N_A)$ (N_A is Avogadro's number) in a cell for a salt-free colloid according to the pointlike model (PL), Bk (for different packing factors), and C-S approaches, and Na^+ with radius $R = 0.358$ nm as the released counterion (see Ref. [37] for all ionic data used in this work). In Fig. 2(a), a less effective screening effect on the particle surface charge is predicted according to C-S in comparison with the other approaches, as evidenced by the enhancement of the equilibrium electric potential at every distance from the particle surface. Also, the higher the packing factor in the Bk formalism, the closer its prediction will be to the PL case. Quite remarkable is the fact that the C-S prediction doubles that of the PL case in the immediacy of the particle surface, which will have important consequences on the electrokinetic properties that will be studied in the next section.

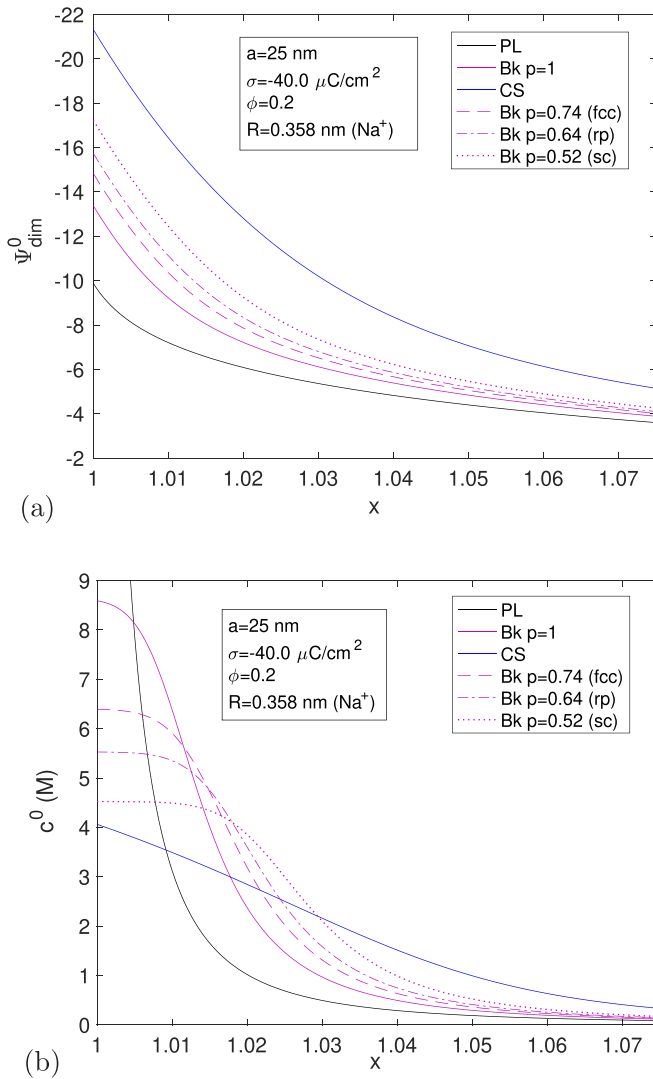


FIG. 2. (a) Dimensionless equilibrium electric potential and (b) molar equilibrium counterion concentration as a function of the dimensionless radial distance $x = r/a$ from the particle center according to the PL, Bk [$p = 1$ (perfect packing), $p = 0.74$ (face-centered cubic packing), $p = 0.64$ (random close packing), $p = 0.523$ (simple cubic packing)], and C-S approaches with $R = 0.358$ nm (Na^+), $a = 25$ nm, $\sigma = -40.0$ $\mu\text{C}/\text{cm}^2$, and $\phi = 0.2$.

It is clearly displayed in Fig. 2(b) that the counterions are forced to occupy regions farther from the particle because of their finite size, thus avoiding high ionic concentrations (as those predicted by the PL case) near the particle surface. A lower counterion concentration close to the particle surface is predicted by the C-S analysis than by the other ones. The larger concentrations of counterions for the C-S case far from the particle surface, mainly for high particle volume fraction and high particle surface charges, will have important consequences on the counterion fluxes surrounding the particles and on the electrophoretic mobility and electrical conductivity. These effects will also be present with the other finite-size approaches, but are magnified with the C-S one. Note in Fig. 2(b) that a counterion concentration plateau is predicted by the Bk formalism at the shortest distances from the particle

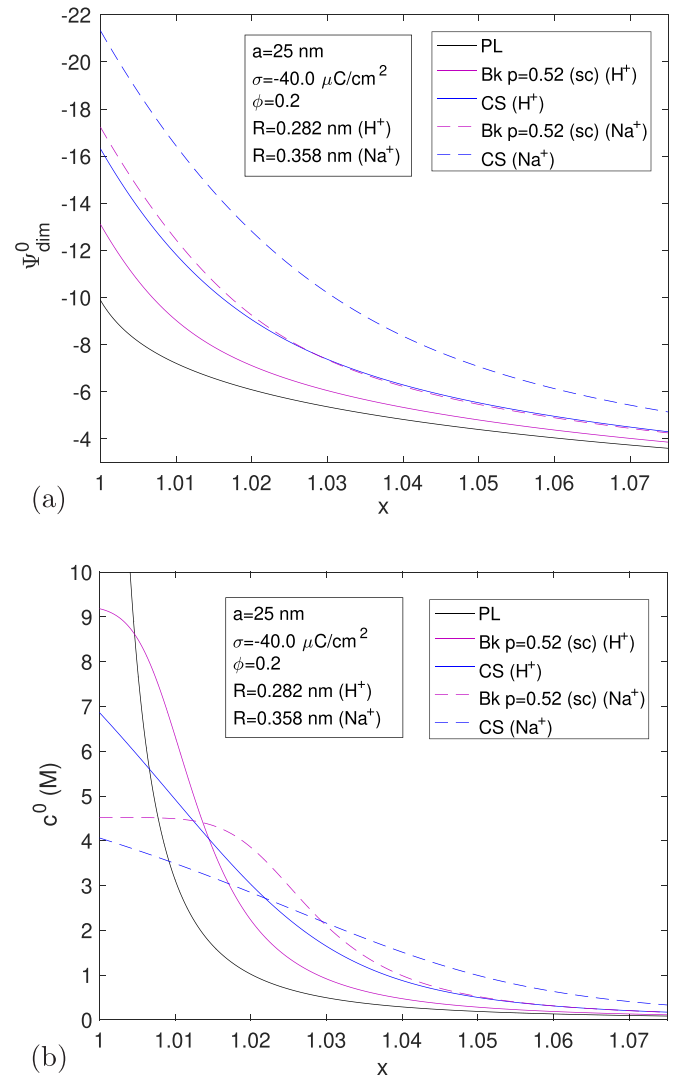


FIG. 3. (a) Dimensionless equilibrium electric potential and (b) molar equilibrium counterion concentration as a function of the dimensionless radial distance $x = r/a$ from the particle center according to the PL, Bk [$p = 0.523$ (simple cubic packing)], and C-S approaches with different counterions: $R = 0.282$ nm (H^+) and $R = 0.358$ nm (Na^+), $a = 25$ nm, $\sigma = -40.0$ $\mu\text{C}/\text{cm}^2$, and $\phi = 0.2$.

surface due to the existence of a maximum concentration allowed for a given packing factor [see Eq. (3)]. Such plateaus are not predicted by the C-S approach, where the counterion concentration displays a monotonous decrease with distance whatever the conditions chosen.

In Fig. 3 we compare the dimensionless equilibrium electrical potential (a) and the equilibrium counterion concentration (b) for different counterion radii: $R = 0.282$ nm (H^+) and $R = 0.358$ nm (Na^+) according to PL (pointlike model), Bk (just for simple cubic packing), and C-S approaches. Figure 3(a) corresponds to the case of the electric potential. For brevity, just the simple cubic packing in the Bk study will be used for the comparison with the C-S predictions. A lower screening effect on particle surface charge is observed with the bigger counterion Na^+ in comparison with that for the smaller H^+ . This effect is shown with both approaches, as evidenced

by the superior values displayed for the Na^+ electric potential at every distance from the particle surface. In addition, the effect is larger for the C-S approach than for the Bk one, as expected. Likewise, note that the trends are closer to the pointlike predictions for the smaller ions H^+ .

In Fig. 3(b) we study the equilibrium counterion concentration as a function of the distance from the particle surface for the different counterions and conditions used in Fig. 3(a). It is observed the expected lower Na^+ counterion concentration close to the particle surface in comparison with that for H^+ counterions because of the bigger size of the former ones. This effect is more pronounced according to the C-S approach: A less compact layer of Na^+ counterions is built in the close region to the particle surface, that extends farther into the solution than in either the Bk or PL cases, due to the larger counterion size of Na^+ counterions.

IV. ELECTROKINETIC EQUATIONS AND BOUNDARY CONDITIONS IN DC AND AC ELECTRIC FIELDS

Let us again consider a spherical particle of radius a , surface charge density σ , mass density ρ_p and relative permittivity ε_{rp} surrounded by a shell of a solution of relative permittivity ε_{rs} with outer radius $b = a\phi^{-1/3}$ (the radius of the cell), and ϕ the particle volume fraction of the colloid. An alternating electric field $\vec{E} \exp(-j\omega t)$ of angular frequency ω is applied to the system. In the stationary state, the particle will move with a velocity $\vec{V}_p \exp(-j\omega t)$ where $\vec{V}_p = u_e \vec{E}$, being u_e the dynamic electrophoretic mobility (the notation u_{edc} will refer to the electrophoretic mobility for the dc limit). A spherical coordinate system (r, θ, φ) is fixed at the center of the particle, and the polar axis ($\theta = 0$) is chosen to be parallel to the applied electric field.

The fundamental equations connecting the electrical potential $\Psi(\vec{r}, t)$, the concentration of counterions $n(\vec{r}, t)$ and their drift velocity $\vec{v}(\vec{r}, t)$, the fluid velocity $\vec{u}(\vec{r}, t)$ and the pressure $P(\vec{r}, t)$ at every point \vec{r} in the system and time t are [38–40]:

$$\nabla^2 \Psi(\vec{r}, t) = -\frac{\rho_{\text{el}}(\vec{r}, t)}{\varepsilon_{\text{rs}} \varepsilon_0}, \quad (23)$$

$$\rho_{\text{el}}(\vec{r}, t) = zen(\vec{r}, t), \quad (24)$$

$$\begin{aligned} \eta_s \nabla^2 \vec{u}(\vec{r}, t) - \nabla P(\vec{r}, t) - \rho_{\text{el}}(\vec{r}, t) \nabla \Psi(\vec{r}, t) \\ = \rho_s \frac{\partial}{\partial t} [\vec{u}(\vec{r}, t) + \vec{V}_p \exp(-i\omega t)], \end{aligned} \quad (25)$$

$$\nabla \cdot \vec{u}(\vec{r}, t) = 0, \quad (26)$$

$$\vec{v}(\vec{r}, t) = \vec{u}(\vec{r}, t) - \frac{1}{\lambda} \nabla \mu(\vec{r}, t), \quad (27)$$

$$\mu(\vec{r}, t) = \mu^\infty + ze\Psi(\vec{r}, t) + k_B T \ln[\gamma(\vec{r}, t) n(\vec{r}, t)], \quad (28)$$

$$\nabla \cdot [n(\vec{r}, t) \vec{v}(\vec{r}, t)] = -\frac{\partial n(\vec{r}, t)}{\partial t}. \quad (29)$$

Equation (23) is Poisson's equation, where $\rho_{\text{el}}(\vec{r}, t)$ is the electric charge density [Eq. (24)]. Equations (25) and (26) are the Navier-Stokes equations for an incompressible fluid flow of viscosity η_s and mass density ρ_s at low Reynolds number in the presence of an electrical body force. Equation (27) derives

from the Nernst-Planck equation for the flow of the counterion species, including the gradient of its electrochemical potential $\mu(\vec{r}, t)$ defined in Eq. (28), and $\lambda = k_B T / D$ its drag coefficient (D is the counterion diffusion coefficient). The $\gamma(\vec{r}, t)$ in Eq. (28) is the nonequilibrium activity coefficient of the counterion that will be assumed to explicitly maintain a similar concentration dependence as either the Carnahan-Starling activity coefficient [see Eq. (1)] or the Bikerman activity coefficient [see Eq. (3)]. Finally, Eq. (29) is the continuity equation for the conservation of the counterion species.

The appropriate boundary conditions are [41]

$$\Psi_p(\vec{r}, t) = \Psi(\vec{r}, t) \text{ at } r = a, \quad (30)$$

$$\varepsilon_{\text{rs}} \nabla \Psi(\vec{r}, t) \cdot \hat{r} - \varepsilon_{\text{rp}} \nabla \Psi_p(\vec{r}, t) \cdot \hat{r} = -\sigma / \varepsilon_0 \text{ at } r = a, \quad (31)$$

$$\vec{u}(\vec{r}, t) = 0 \text{ at } r = a, \quad (32)$$

$$\vec{v}(\vec{r}, t) \cdot \hat{r} = 0 \text{ at } r = a, \quad (33)$$

$$\vec{\omega}(\vec{r}, t) = \nabla \times \vec{u}(\vec{r}, t) = 0 \text{ at } r = b, \quad (34)$$

$$n(\vec{r}, t) - n^0(r) = 0 \text{ at } r = b, \quad (35)$$

$$\Psi(\vec{r}, t) - \Psi^0(r) = -\vec{E} \cdot \vec{r} \exp(-j\omega t) \text{ at } r = b. \quad (36)$$

We will also make use of an integral condition that will be determinant for deriving the electrophoretic mobility:

$$\langle \rho_m \vec{u}'(\vec{r}, t) \rangle = \frac{1}{V_{\text{cell}}} \int_{V_{\text{cell}}} \rho_m \vec{u}'(\vec{r}, t) dV = 0 \quad (37)$$

with \vec{u}' being the local velocity with respect to a laboratory reference system, ρ_m is the local mass density and V_{cell} the volume of the unit cell. In summary, the boundary conditions imposed at the particle surface are expressed by Eq. (30), that stands for the continuity of the electric potential, $\Psi_p(\vec{r}, t)$ is the potential inside the particle; Eq. (31), which represents the discontinuity of the normal component of the displacement vector (\hat{r} is the radial unit vector of the spherical coordinate system); Eq. (32), that indicates that the fluid is at rest at the particle surface in the reference system fixed to the particle; Eq. (33), which stands for the impossibility of counterions to penetrate the solid particle. In addition, at the outer surface of the cell the chosen boundary conditions are given by Eq. (34), which stands for the Kuwabara boundary condition of null vorticity $\vec{\omega}$ for the fluid velocity; Eqs. (35) and (36), that are the Shilov-Zharkikh-Borkovskaya boundary conditions [33] for the perturbed concentration of counterions and perturbed electric potential in such surface; and the integral condition in Eq. (37), that according to O'Brien [42], imposes that the macroscopic momentum per unit volume of the colloid is zero, allowing us to obtain the dynamic electrophoretic mobility. Finally, the equation of motion of the unit cell with the net force acting on it will permit us to close the problem [41,43].

V. LINEAR PERTURBATION SCHEME AND LINEARIZED ELECTROKINETIC EQUATIONS AND BOUNDARY CONDITIONS

In this work we are interested in the linear response of the colloid in the presence of low-strength electric fields, or, equivalently, low Péclet number, Pe , regime. Recall that low values of Pe mean that the system remains close to equilibrium during transport, as it is given by the ratio between advection and diffusion characteristic times. In the case of particles undergoing electrophoresis in the presence of an electric field, the Péclet number can be calculated as [44]:

$$Pe = \frac{a u_e E}{D}, \quad (38)$$

where the particle diffusion coefficient D is given by $D = k_B T / 6\pi\eta_s a$. Using a value of 25 nm for the particle radius, it is found that $Pe \sim 10^{-4} E$. For the typical field strength values used in electrophoretic determinations ($E \sim 1000$ – 2000 V/m) and the maximum values of the electrophoretic mobility obtained in this study ($\sim 10 \times 10^{-8} \text{ m}^2 \text{ V}^{-1} \text{ s}^{-1}$, see below), the Péclet number would be in the order of 0.1. Even lower Péclet numbers are estimated for the low fields used in dielectric measurements (100 V/m). Regarding the fulfillment of the low-Péclet condition for increasing electric fields, the limit would be around 1 – 2×10^4 V/m, and these fields are never used in electrokinetics in aqueous solutions.

In this work we are interested in the linear response of the colloid in the presence of low-strength electric fields. Thus, when a low-strength alternating electric field $\vec{E} \exp(-j\omega t)$ is applied to the system, a first-order perturbation scheme can be applied to the out-of-equilibrium situation. Each quantity $X(\vec{r}, t)$ is expressed as the summation of its equilibrium value $X^0(r)$ plus a field-induced linear perturbation $\delta X(\vec{r}) \exp(-j\omega t)$. We note that the equilibrium fluid velocity and ionic drift velocity are taken as zero, so that $\vec{u}(\vec{r}, t)$ and $\vec{v}(\vec{r}, t)$ are actually pure field-induced linear perturbations.

The spherical symmetry of the problem permits us to express [38]:

$$\begin{aligned} \delta \vec{u}(\vec{r}) &= \left[-\frac{2h}{r} E \cos \theta, \frac{1}{r} \frac{d(rh)}{dr} E \sin \theta, 0 \right], \\ \delta \mu(\vec{r}) &= -ze\phi(r)E \cos \theta, \\ \delta \Psi(\vec{r}) &= -Y(r)E \cos \theta, \\ \delta \Psi_p(\vec{r}) &= -Y_p(r)E \cos \theta, \end{aligned} \quad (39)$$

$$\delta P(\vec{r}) = P(r)E \cos \theta,$$

in terms of some radial functions $h(r)$, $\phi(r)$, $Y(r)$, $Y_p(r)$, and $P(r)$, that contain information about the field-induced linear perturbations. Also, as it is shown below, it is easy to demonstrate that

$$\begin{aligned} \delta n(\vec{r}) &= \frac{n^0(r) \Lambda(r)}{k_B T} [\delta \mu(\vec{r}) - ze\delta \Psi(\vec{r})] \\ &= -\frac{ze n^0(r) \Lambda(r)}{k_B T} [\phi(r) - Y(r)] E \cos \theta. \end{aligned} \quad (40)$$

The $\Lambda(r)$ function in Eq. (40) is completely known because it only involves known quantities once the equilibrium MPB equation is solved [Eqs. (18)–(21), see the Appendix for

details]. For the derivation of Eq. (40), it has been assumed that out of equilibrium the electrochemical potential of counterions can be expressed in a similar way as in equilibrium [cf. Eqs. (1), (3), and (28)] except that the argument now becomes (\vec{r}, t) .

From this, it can be demonstrated for linear perturbations that

$$\begin{aligned} \gamma(\vec{r}, t) n(\vec{r}, t) &= \gamma^0(r) n^0(r) \left\{ 1 + \left[\frac{\delta n(\vec{r})}{n^0(r)} + \frac{\delta \gamma(\vec{r})}{\gamma^0(r)} \right] \exp(-j\omega t) \right\} \end{aligned} \quad (41)$$

and

$$\delta \mu(\vec{r}) = ze\delta \Psi + k_B T \left[\frac{\delta n(\vec{r})}{n^0(r)} + \frac{\delta \gamma(\vec{r})}{\gamma^0(r)} \right]. \quad (42)$$

On the other hand and according to the first-order perturbation procedure, we approximately have

$$\begin{aligned} \ln[\gamma(\vec{r}, t)] &= \ln[\gamma^0(r) + \delta \gamma(\vec{r}) \exp(-j\omega t)] \\ &= \ln \left\{ \gamma^0(r) \left[1 + \frac{\delta \gamma(\vec{r})}{\gamma^0(r)} \exp(-j\omega t) \right] \right\} \\ &= \ln[\gamma^0(r)] + \ln \left[1 + \frac{\delta \gamma(\vec{r})}{\gamma^0(r)} \exp(-j\omega t) \right] \\ &\approx \ln[\gamma^0(r)] + \frac{\delta \gamma(\vec{r})}{\gamma^0(r)} \exp(-j\omega t). \end{aligned} \quad (43)$$

By using again the first-order perturbation scheme with the $\gamma(\vec{r}, t)$ function, and taking its natural logarithm we finally obtain, after equating with Eq. (43), the result:

$$\frac{\delta \gamma(\vec{r})}{\gamma^0(r)} = \left[\frac{1}{\Lambda(r)} - 1 \right] \frac{\delta n(\vec{r})}{n^0(r)}, \quad (44)$$

where $\Lambda(r)$ stands for either $\Lambda(r)_{\text{CS}}$ or $\Lambda(r)_{\text{BK}}$, that were previously defined in Eqs. (19) and (20), respectively. Finally, substituting Eq. (44) in Eq. (42) we find:

$$\delta \mu(\vec{r}) = ze\delta \Psi + \frac{k_B T}{\Lambda(r)} \left[\frac{\delta n(\vec{r})}{n^0(r)} \right], \quad (45)$$

from which Eq. (40) is immediately derived.

The linearized electrokinetic equations of the full set expressed in Eqs. (24)–(29), are as follows. The linearized continuity equation for the counterions become

$$\begin{aligned} \mathcal{L}\phi(r) &= - \left\{ \frac{j\omega\lambda}{k_B T} [\phi(r) - Y(r)] - \frac{e}{k_B T} \left(\frac{d\Psi^0}{dr} \right) \right. \\ &\quad \left. \times \left[z \frac{d\phi(r)}{dr} - \frac{2\lambda}{er} h(r) \right] \right\} \Lambda(r), \end{aligned} \quad (46)$$

where \mathcal{L} means the mathematical linear differential operator:

$$\mathcal{L} \equiv \frac{d^2}{dr^2} + \frac{2}{r} \frac{d}{dr} - \frac{2}{r^2}. \quad (47)$$

The out-of-equilibrium Poisson equation after linearizing becomes

$$\mathcal{L}Y(r) = -\frac{z^2 e^2 n^0(r)}{\epsilon_{\text{rs}} \epsilon_0 k_B T} [\phi(r) - Y(r)] \Lambda(r) \quad (48)$$

and the linearized Navier-Stokes equation turns out to be

$$\mathcal{L}\left[\mathcal{L}h(r) + \frac{j\omega\rho_s}{\eta_s}h(r)\right] = -\frac{z^2e^2n^0(r)}{k_B T \eta_s r} \left[\frac{d\Psi^0(r)}{dr}\right] \phi(r) \Lambda(r). \quad (49)$$

As mentioned, $\Lambda(r) \rightarrow 1$ stands for the pointlike case, and Eqs. (46), (48), and (49) become the already-known linearized electrokinetic equations for a salt-free colloid with pointlike counterions that were derived in a previous paper [45]. By using the perturbation scheme and the symmetry conditions, the linearized version of the boundary conditions described in Eq. (30) and Eq. (36) can finally be expressed as:

$$h(a) = 0, \quad (50)$$

$$\frac{dh}{dr}(a) = 0, \quad (51)$$

$$\frac{d^2h}{dr^2}(b) + \frac{2}{b} \frac{dh}{dr}(b) - \frac{2}{b^2}h(b) = 0, \quad (52)$$

$$\frac{d\phi}{dr}(a) = 0, \quad (53)$$

$$\phi(b) = b, \quad (54)$$

$$\frac{dY}{dr}(a) - \frac{\varepsilon_{rp}}{\varepsilon_{rs}} \frac{Y(a)}{a} = 0, \quad (55)$$

$$Y(b) = b. \quad (56)$$

Also the linearized version of the integral condition in Eq. (37) allows us to calculate the electrophoretic mobility as [1]:

$$u_e = \frac{2h(b)}{b} \frac{1}{\left[1 + \left(\frac{\rho_p - \rho_s}{\rho_s}\right)\phi\right]}. \quad (57)$$

In alternating electric fields, the latter ‘‘dynamic or ac’’ electrophoretic mobility is commonly expressed in terms of its real and imaginary components: $u_e = u'_e + ju''_e$.

Finally, the linearized version of the net force acting on the unit cell closes the problem [1,41,43]:

$$\begin{aligned} & \frac{d^3h}{dr^3}(b) + \frac{1}{b} \frac{d^2h}{dr^2}(b) - \frac{6}{b^2} \frac{dh}{dr}(b) + \frac{6}{b^3}h(b) - \frac{j\omega\rho_s}{\eta_s} \\ & \times \left[\frac{h(b)}{b} - u_e \frac{(\rho_p - \rho_s)}{\rho_s} \phi - \frac{dh}{dr}(b) \right] \\ & = \frac{\rho_{el}^0(b) Y(b)}{b\eta_s}. \end{aligned} \quad (58)$$

Concerning the complex electrical conductivity $K^*(\omega)$ of the colloid, it is usually derived from the linear relation between macroscopic electric current density $\vec{i}(\vec{r}, t)$ and macroscopic electric field $(-\nabla\Psi(\vec{r}, t))$. According to the cell model approach, a given macroscopic property is expressed by a volume average of its corresponding local

property in the volume of a cell V_{cell} :

$$\begin{aligned} \langle \vec{i}(\vec{r}, t) \rangle &= \frac{1}{V_{\text{cell}}} \int_{V_{\text{cell}}} \vec{i}(\vec{r}, t) dV \\ &= K^*(\omega) \langle -\nabla\Psi(\vec{r}, t) \rangle \\ &= K^* \frac{1}{V_{\text{cell}}} \int_{V_{\text{cell}}} [-\nabla\Psi(\vec{r}, t)] dV, \end{aligned} \quad (59)$$

where the local current density $\vec{i}(\vec{r}, t)$ is defined as:

$$\vec{i}(\vec{r}, t) = \rho_{el}(\vec{r}, t)\vec{v}(\vec{r}, t) - \frac{\partial}{\partial t}[\varepsilon_{rs}\varepsilon_0\nabla\Psi(\vec{r}, t)]. \quad (60)$$

Details for the calculation of the complex electrical conductivity $K^*(\omega)$ can be found in the Supplementary Information File of Ref. [1]. Thus, $K^*(\omega)$ turns out to be

$$\begin{aligned} K^*(\omega) &= \left\{ \frac{z^2e^2n^0(b)}{\lambda} \frac{d\phi}{dr}(b) - zen^0(b) \frac{2h(b)}{b} \right. \\ & \left. - j\omega\varepsilon_0\varepsilon_{rs} \frac{dY}{dr}(b) \right\} \frac{b}{Y(b)}. \end{aligned} \quad (61)$$

The complex relative permittivity $\varepsilon_r^*(\omega) = \varepsilon'_r(\omega) + j\varepsilon''_r(\omega)$ is usually defined from the complex electrical conductivity by the equation:

$$K^*(\omega) = K_{\text{dc}} - j\omega\varepsilon_0\varepsilon_r^*(\omega), \quad (62)$$

where $K_{\text{dc}} = K^*(\omega = 0)$. Separating real and imaginary parts we finally obtain:

$$\varepsilon'_r(\omega) = -\frac{\text{Im}[K^*(\omega)]}{\omega\varepsilon_0}, \quad (63)$$

$$\varepsilon''_r(\omega) = \frac{\text{Re}[K^*(\omega)] - K_{\text{dc}}}{\omega\varepsilon_0}. \quad (64)$$

VI. SOME NUMERICAL RESULTS IN DC AND AC ELECTRIC FIELDS

A. dc results

In Fig. 4 we study the effect of the counterion size on the dimensionless electrophoretic mobility $u_{e\text{DC dim}}$ [Fig. 4(a)], and the electrical conductivity K_{dc} [Fig. 4(b)], as a function of the particle surface charge density at fixed particle volume fraction and Na^+ (radius $R = 0.358$ nm) as the released counterion. The dimensionless mobility is defined as follows:

$$u_{e\text{DC dim}} = \frac{3\eta_s e}{2\varepsilon_{rs}\varepsilon_0 k_B T} u_{e\text{dc}}. \quad (65)$$

In Fig. 4(a), the electrophoretic mobility-charge density plot evidences the well-known counterion condensation effect. As it was previously mentioned, for salt-free colloids a layer of counterions condenses onto the particle surface once the surface charge density surpasses a characteristic onset for the condensation [8,15,46]. Beyond it, the mobility hardly changes on further increasing the particle surface charge. This effect is clearly shown in Fig. 4(a) whatever the finite-size formalism chosen, or even when no size at all is considered for the counterions (PL case). What is more remarkable in our study is the fact that the mobility in the high-surface-charge region is larger for the C-S case in comparison with the other predictions. This can be related to the lower screening

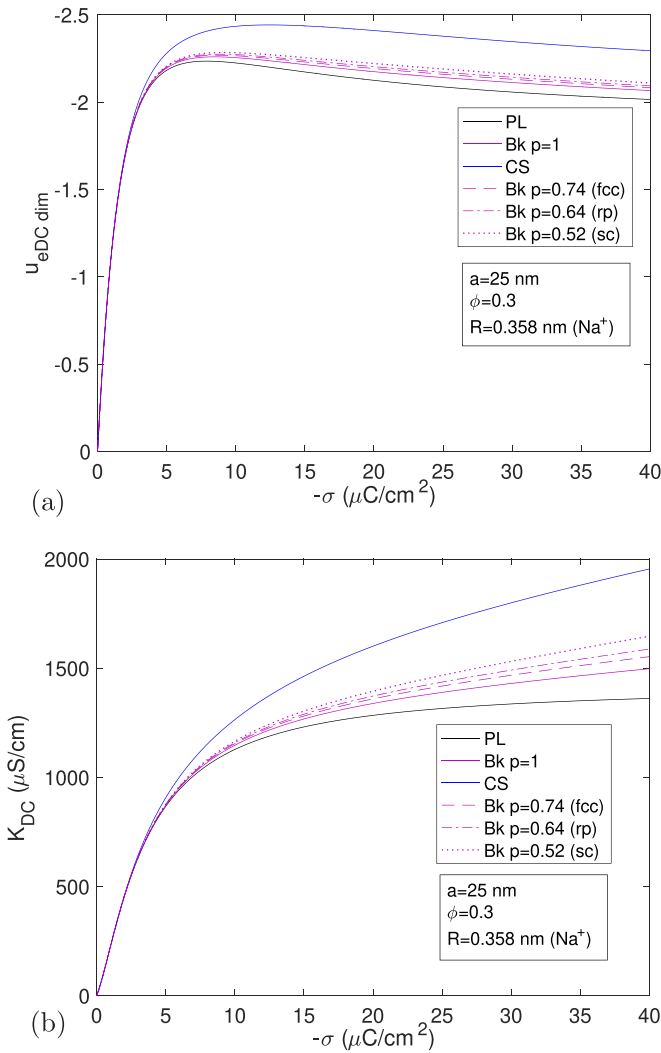


FIG. 4. (a) Dimensionless dc electrophoretic mobility and (b) dc electrical conductivity as a function of particle surface charge density according to the PL, Bk [$p = 1$ (perfect packing), $p = 0.74$ (face-centered cubic packing), $p = 0.64$ (random close packing), $p = 0.523$ (simple cubic packing)], and C-S approaches with $R = 0.358 \text{ nm (Na}^+)$, $a = 25 \text{ nm}$, and $\phi = 0.3$.

effect on particle charge due to the shift of the main region of counterion excess to farther distances from the surface, in comparison with Bk or PL cases. The final result is a modification of the counterion fluxes in the cell affecting relaxation and retardation forces on the particle because of the changes on the electrical body force acting on the fluid. It has been shown that the overall effect is a diminution of the braking effect on the particle motion, leading consequently to an increase of the electrophoretic mobility at high particle surface charges [36,47].

In Fig. 4(b) it is observed a larger dc conductivity according to C-S at high particle charges than those corresponding to the other finite-size approaches. Two different trends of the conductivity are clearly distinguished in the figure. At low particle surface charges, the conductivity linearly increases with particle charge, until the onset for the condensation is attained. A further increase of particle charge only feeds

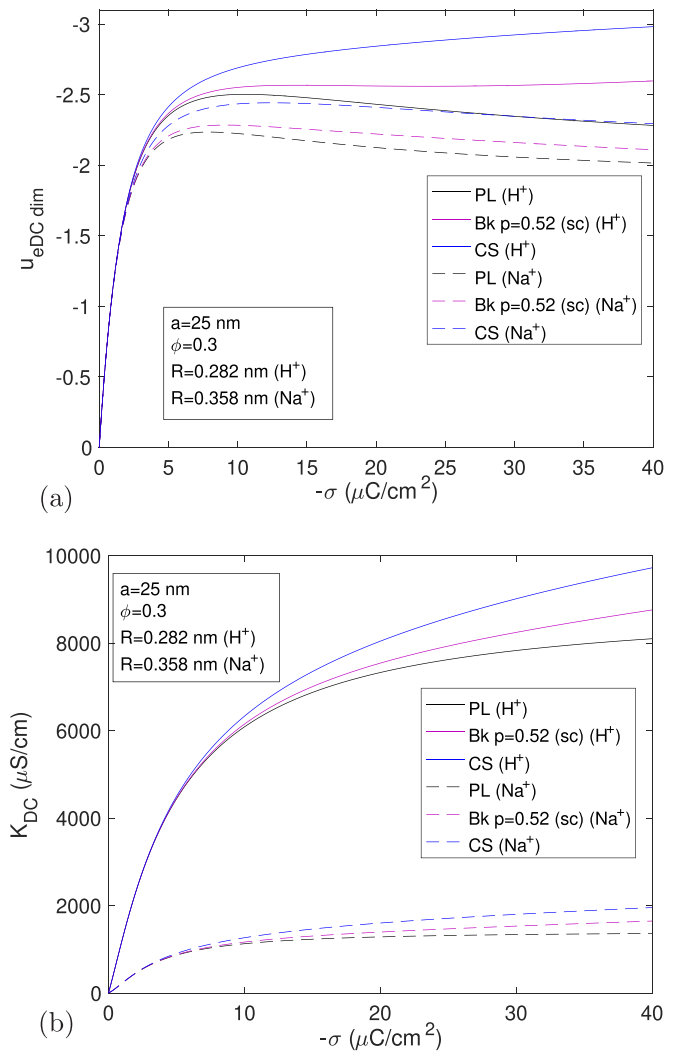


FIG. 5. (a) Dimensionless dc electrophoretic mobility and (b) dc electrical conductivity as a function of particle surface charge density according to the PL, Bk [$p = 0.523$ (simple cubic packing)], and C-S approaches with different counterions: $R = 0.282 \text{ nm (H}^+)$ and $R = 0.358 \text{ nm (Na}^+)$, $a = 25 \text{ nm}$, and $\phi = 0.3$.

the condensate layer, leaving the diffuse layer virtually unchanged, provoking a diminution of the growth rate of the PL conductivity. This classical effect is less pronounced when counterions are allowed to have finite size. As an example, a comparison between C-S and PL conductivity predictions at the highest particle charge displayed in Fig. 4(b) reflects a 30% increase of C-S over the PL prediction. The enhancement (favored by the more gradual decrease with distance of ion concentration in the CS model, see Fig. 2) of the counterion fluxes at the farther regions of the cell where the advective contributions are more important, leads to an increase of the corresponding volume average of the local electric current density in the cell at every particle charge, and therefore, of the electrical conductivity.

In Fig. 5 we show the surface charge density study of (a) the dimensionless dc electrophoretic mobility and (b) the dc electrical conductivity, for two different counterion radii. For simplicity, just a packing factor in the Bikerman study, the

simple cubic packing, has been considered in the comparison. It is first observed the well-known effect of the different counterion diffusion coefficients (a factor of nearly 7 larger in the case of H^+ as compared to Na^+) on the electrokinetic behavior of the particles. It must be noted that the electrophoretic motion is the result of the action of the field on both the particles and the ions, and the model always considers as different, ions with different diffusion coefficients even when they are assumed to be point charges, and consequently no excluded-volume restrictions are imposed on their concentration at any point of the system. This manifests in the different mobility values for H^+ and Na^+ in the PL case. Furthermore, the predicted mobility is larger for both C-S and Bk approaches, whichever the ion considered, a consequence of the fact that the diffuse layer is more populated in counterions. The difference between PL (H^+) and C-S (H^+) is, however, larger than that between PL (Na^+) and C-S (Na^+).

Concerning Fig. 5(b), a huge difference in electrical conductivity can be observed when changing the species of counterions regardless of the finite-size approach. The difference between the diffusion coefficients of both ions is primarily responsible for the changes shown in conductivity. The effect on the dc conductivity increase grows in the sequence C-S > Bk > PL whatever the counterion species, and it is obviously more prominent at high particle charges, as it was previously mentioned concerning Fig. 4(b).

In Fig. 6 we show similar studies as those in Fig. 4 but as a function of the particle volume fraction at fixed particle surface charge density. In Fig. 6(a) it is shown that one of the most outstanding effects of ion size on the electrophoretic mobility is that this quantity may increase with particle concentration in the high concentration limit. This effect is classically prohibited (see the PL case) due to both the expected increase of the hydrodynamic particle-particle interactions and the diminution of the effective particle charge due to the reduction of the liquid volume of the cell available to counterions as the particle volume fraction grows. In this situation, a greater number of counterions are confined in a smaller liquid region. Consequently, the mobility decreases, as clearly shown in Fig. 6(a) for the PL case. But the mobility behavior changes in the high-volume-fraction region when counterions are allowed to have finite size. It is observed an increase of the mobility in spite of the above-mentioned opposing effects on it, and it is more notorious for the C-S approach. The region of the cell in which ions are distributed is wider in the latter model, and this produces an increase of electro-osmotic fluxes which manifest in larger mobility. This contribution overcomes the braking due to particle-particle interactions [36].

As regards the effects of the finite counterion size on the dc electrical conductivity as a function of particle volume fraction displayed in Fig. 6(b), one finds a common increasing behavior of the conductivity for all finite-size approaches including the PL one, the most notable effect being predicted for C-S conditions. When the counterions are allowed to have finite size, their concentration decreases at a slower rate as the separation from particle surface increases in comparison with the sharp decreasing concentration behavior shown by the PL case [see Fig. 2(b)]. Thus, local electric conduction in a less constrained liquid region as we move farther from the

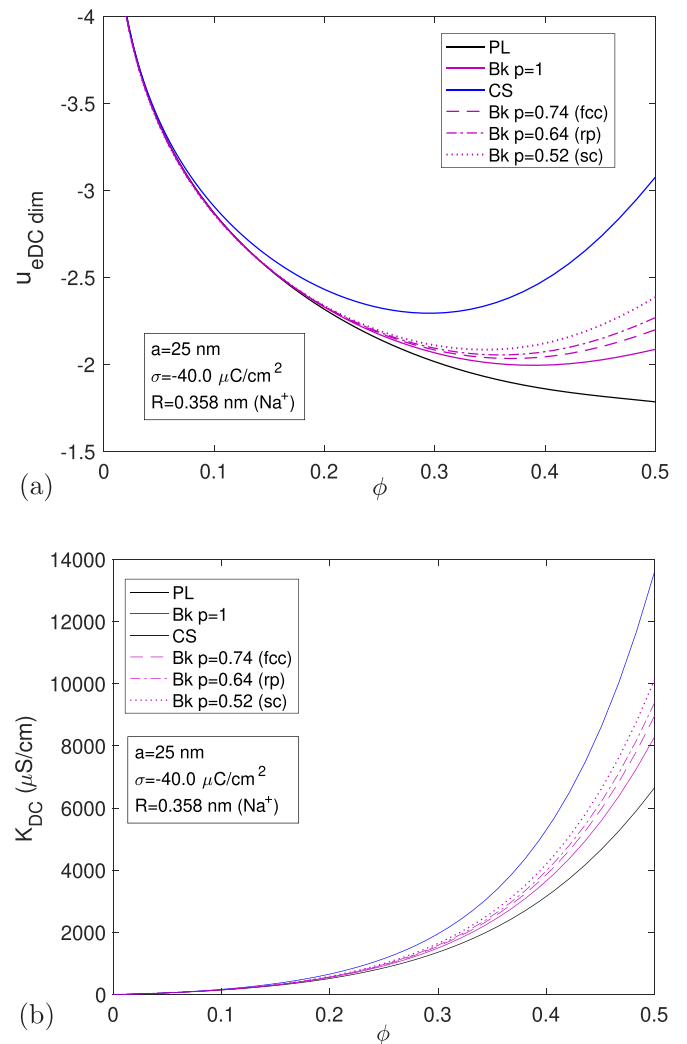


FIG. 6. (a) Dimensionless dc electrophoretic mobility and (b) dc electrical conductivity as a function of particle volume fraction according to the PL, Bk [$p = 1$ (perfect packing), $p = 0.74$ (face-centered cubic packing), $p = 0.64$ (random close packing), $p = 0.523$ (simple cubic packing)], and C-S approaches with $R = 0.358$ nm (Na^+), $a = 25$ nm, and $\sigma = -40.0 \mu\text{C}/\text{cm}^2$.

particle surface is favored by the enhancement of the number of finite-size mobile counterions in it, that leads to the increase of the overall electric current.

Analogously, in Fig. 7 we show the particle concentration study of (a) the dimensionless dc electrophoretic mobility and (b) the dc electrical conductivity for two different counterion radii for comparison. Again and for simplicity, just the simple cubic packing factor in the Bikerman study will be considered in the comparison. As in Fig. 6(a), the effects of the finite size on increasing the mobility are larger with the C-S approach, and even more when the more rapid H^+ counterions are chosen, as clearly seen in Fig. 7(a). The mobility increase with volume fraction predicted by finite ion size models at high particle concentrations is magnified if we apply C-S conditions, as also described in Fig. 7(a). Finally, as it was shown in Fig. 6(b) for the Na^+ counterions, a clear increase of the dc conductivity with volume fraction is also observed with

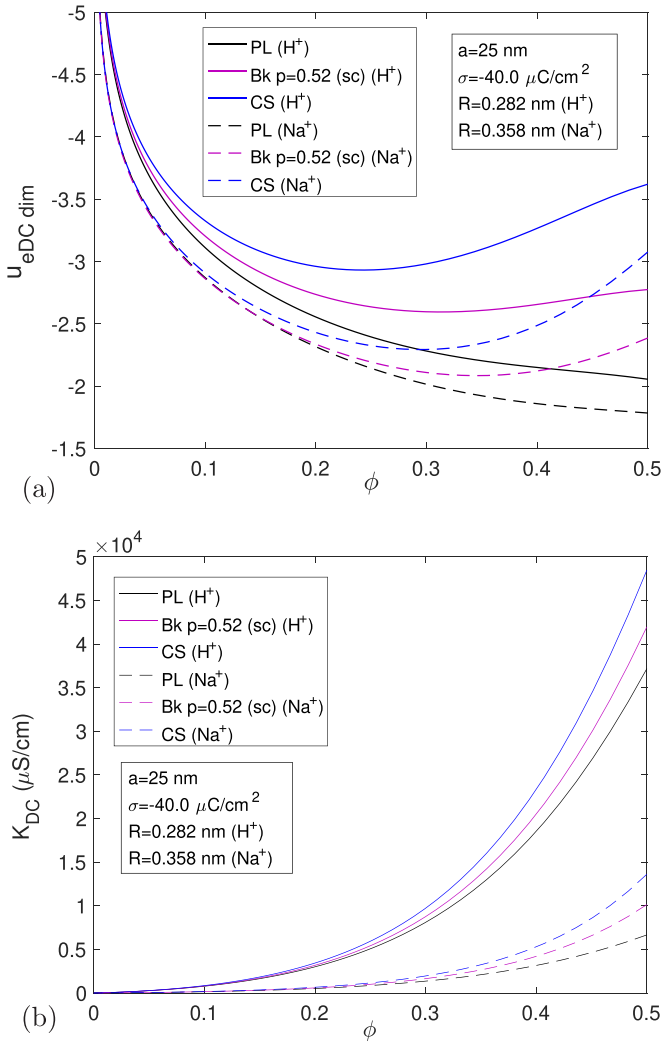


FIG. 7. (a) Dimensionless dc electrophoretic mobility and (b) dc electrical conductivity as a function of particle volume fraction according to the PL, Bk [$p = 0.523$ (simple cubic packing)], and C-S approaches with different counterions: $R = 0.282$ nm (H^+) and $R = 0.358$ nm (Na^+), $a = 25$ nm, and $\sigma = -40.0 \mu C/cm^2$.

the H^+ counterions in Fig. 7(b). Again, the larger diffusion coefficient of H^+ over that of Na^+ can justify the results. As expected, it is the C-S approach which gives the largest conductivity predictions. It must be pointed out that the effect of the finite size of counterions leads to huge conductivity increases whatever the counterion species at high particle concentrations. In order to understand the differences between C-S or Bk and PL models, arguments based on the predicted wider region of ion distribution in the former can again be used for the present results.

B. ac results

In the following, we will study the effects of the finite size of the counterions (C-S, Bk, and PL) approaches on the electrokinetic and dielectric response of a concentrated salt-free colloid subjected to an alternating electric field, in terms of the complex electrophoretic mobility (dynamic mobility) of a particle, and the complex relative permittivity of

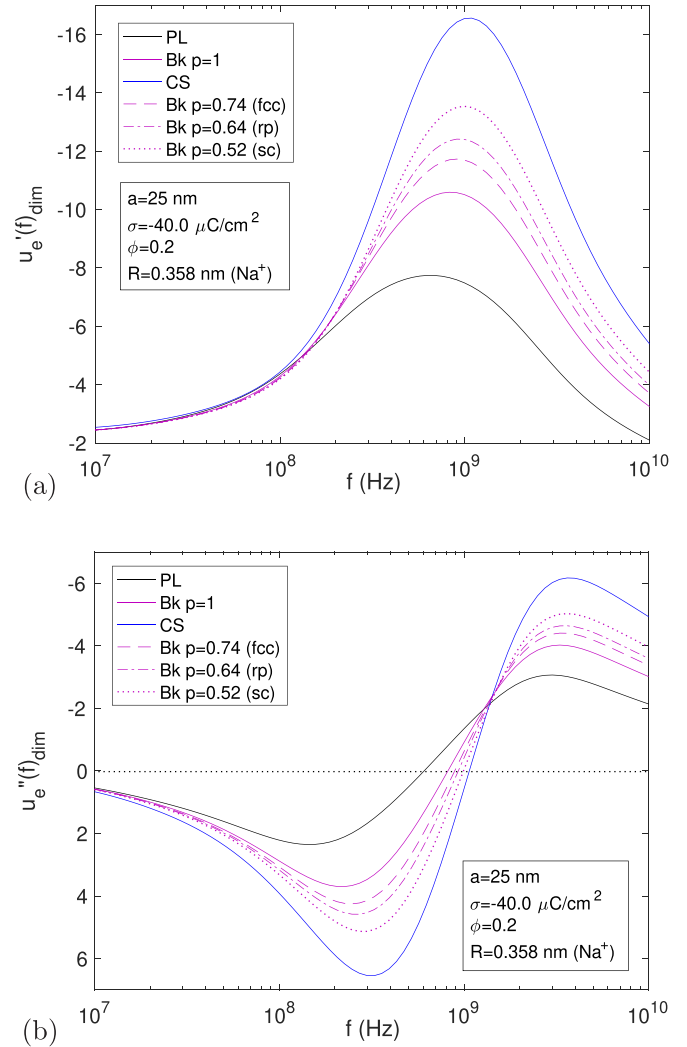


FIG. 8. (a) Dimensionless real part and (b) dimensionless imaginary part of the dynamic electrophoretic mobility as a function of frequency for salt-free colloids according to the PL, Bk [$p = 1$ (perfect packing), $p = 0.74$ (face-centered cubic packing), $p = 0.64$ (random close packing), $p = 0.523$ (simple cubic packing)], and C-S approaches with $R = 0.358$ nm (Na^+), $a = 25$ nm, $\sigma = -40.0 \mu C/cm^2$, and $\phi = 0.2$.

the colloid. Figures 8 and 9 show the real and imaginary parts of the dimensionless dynamic electrophoretic mobility $u_{e,dim} = u_e'_{dim} + ju_e''_{dim}$ [same scaling factor as that in Eq. (65)], and the real and imaginary parts of the complex relative permittivity $\epsilon_r^* = \epsilon_r' + j\epsilon_r''$, respectively, as a function of frequency assuming $p = 1$ (perfect packing), $p = 0.74$ (face-centered cubic packing), $p = 0.64$ (random close packing), and $p = 0.523$ (simple cubic packing) in the Bk model, and ionic radius $R = 0.358$ nm (Na^+), particle radius $a = 25$ nm, particle surface charge density $\sigma = -40.0 \mu C/cm^2$, and particle volume fraction $\phi = 0.2$. As regards Fig. 8(a), a huge elevation of the high-frequency mobility is observed whatever the model used for counterions: Recall that an external electric field induces an electric dipole because of the rearrangement of the countercharge surrounding the particle (this is often called Maxwell-Wagner-O'Konski (MWO) polarization

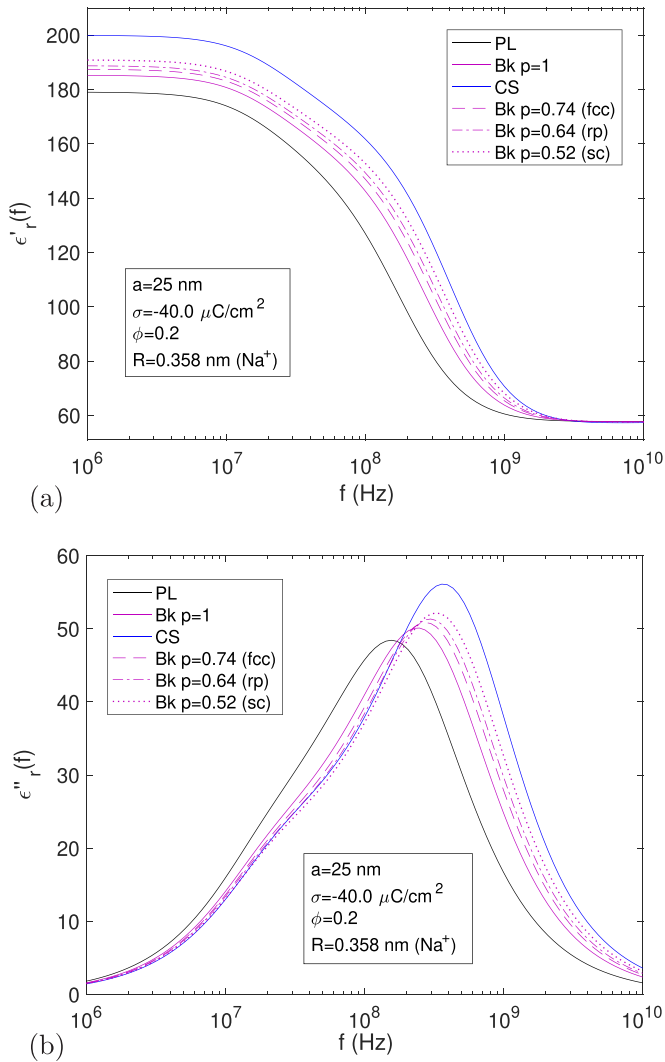


FIG. 9. (a) Real part and (b) imaginary part of the complex relative permittivity as a function of frequency for salt-free colloids according to the PL, Bk [$p = 1$ (perfect packing), $p = 0.74$ (face-centered cubic packing), $p = 0.64$ (random close packing), $p = 0.523$ (simple cubic packing)], and C-S approaches with $R = 0.358$ nm (Na^+), $a = 25$ nm, $\sigma = -40.0$ $\mu\text{C}/\text{cm}^2$, and $\phi = 0.2$.

process [39]), reducing the strength of the tangential component of the electric field close to the particle and thus decreasing the mobility. In consequence, when the frequency is further increased, when the MWO relaxes, then the electrophoretic mobility increases. In the case of interest here, salt-free colloids, another Maxwell-Wagner process comes into play for even higher frequencies, and this can be associated to the polarization of the counterion condensation layer [13,15,36]. We call this an MWC process, and it can be linked to a shorter characteristic length (the thickness of the condensate) than the classical MWO process (its length is the diffuse layer thickness). In the data shown in Fig. 8(a) there is no clear distinction between both phenomena (MWO and MWC), but rather a wide relaxation band extending over more than one decade in frequency. The mobility increase is predicted to be larger when the finite size of the counterions is considered. The highest rise is

obtained with the C-S approach (the maximum C-S mobility doubles the PL one at 1 GHz).

Note, in addition, that the dynamic mobility does not remain constant above that point. It so happens that at very large frequencies the mobility tends to decrease when the so-called inertia region is reached, as in this frequency region particles and fluid are unable to follow the rapid oscillations of the electric field. In summary, what we observe in Fig. 8(a) is a global increase of the mobility as frequency increases due to the relaxation of both MW processes (very close in frequency in this example, as will be confirmed by dielectric dispersion data, see below), and the final decrease because of the inertia at the highest frequencies explored.

The imaginary part of the dimensionless electrophoretic mobility is plotted as a function of frequency in Fig. 8(b) for the same cases considered in Fig. 8(a). This representation of the imaginary part of the mobility versus frequency is very useful in identifying the different relaxation frequencies [39,45]: A maximum in such property along the frequency spectrum (a minimum in the figure, because the y axis is inverted) marks the relaxation frequency of a single MW relaxation process. The relaxation frequency corresponds also to the inflection point in the real part of the mobility-frequency curve in Fig. 8(a). In our case we have two MW relaxation processes, MWO and MWC, that are very close in frequency, as mentioned, showing a global minimum. A shift can be observed in the MW relaxation frequency, which increases when the finite ion volume is taken into consideration. This behavior will be more clearly observed in the permittivity, and it will be discussed below. On the other hand, the frequency of the maximum observed at higher frequencies (recall that it is a high-frequency minimum in reality) indicates the frequency of the inertial relaxation of the particle motion. In Fig. 9(a) the real part of the complex relative permittivity ϵ'_r as a function of frequency of the electric field is displayed. There is an increase of ϵ'_r above pointlike descriptions along the whole frequency spectrum when ion-size effects are taken into account. The effect of increasing ϵ'_r is larger for the C-S approach in comparison with that of Bikerman whatever the packing factor chosen. It has been argued that larger induced electric dipole moments are formed when counterions have finite size because they cannot accumulate near the particle surface at such high concentrations as in the PL case because of the excluded counterion volume. This leads to larger polarizable structures (charge particle + countercharge in solution) and a higher dielectric response. Note that the two MW processes above mentioned are to some extent distinguishable in the dielectric spectra, in the form of a shoulder in the curves, confirming that the two frequencies are quite close to each other. Interestingly, the two processes are not observable as separate ones in the case of mobility spectra (Fig. 8), demonstrating the great sensitivity of dielectric dispersion to the dynamic processes of the double layer.

This is confirmed by the imaginary part of the complex relative permittivity shown in Fig. 9(b). In this figure the two MW relaxation processes (peaks of ϵ''_r in this frequency spectrum) can reasonably be appreciated. Also, there is a large response when counterions are allowed to have finite size, a bit more relevant for the C-S formalism. As it has been reported [40], there is also observed a frequency shift to larger

frequencies of the MWC relaxation frequency when finite-size predictions are compared to the PL one, clearly visible in Fig. 9(b). This frequency shift has been related to the increase of both the electrical conductivity, already pointed out in previous figures, and the width of the condensate layer for finite-size ions [40]. In fact, the MWC relaxation frequency ω_{MWC} is approximately given, in the case of Bk models by [36]:

$$\omega_{\text{MWC}} = \frac{2z^2 e^2 n^{\text{max}} \delta (1 - \phi)}{\varepsilon_0 \varepsilon_{\text{rs}} a \lambda (2 + \phi)}, \quad (66)$$

which is proportional to the product $n^{\text{max}} \delta$, being δ the thickness of the condensate. For C-S calculations n^{max} is not well defined; we will estimate it as the counterion concentration close to the particle surface. As it can be deduced from Sec. II, n^{max} decreases and the condensate thickness δ increases with the diminution of the packing factor in the Bk study, although the product $n^{\text{max}} \delta$ may augment [36]. This could occur if despite the decrease in n^{max} with the packing factor, the width of the condensate δ grew at a higher rate [40]. This effect can explain the frequency shift in Fig. 9(b). Note that the counterion concentration in the very close region to the particle surface according to C-S is always smaller than those predicted by the Bk approach, whereas the width of the condensate is clearly larger for the C-S case [see Figs. 2(b) and 3(b)]. This explains the apparent larger shift to higher frequencies of the C-S imaginary part of the complex permittivity observed in Fig. 9(b), in accordance with Eq. (66).

Analogously, in Figs. 10 and 11 similar studies as those shown in Figs. 8 and 9 can be found, but for two different counterion radii. Again and for brevity, only the Bikerman study with the simple cubic packing factor has been considered in the comparison. In Figs. 10(a) and 10(b) we compare the finite-size effects, according to the different models, on the dimensionless mobility. It is found that, similarly to our findings of dc mobility, the real part of the dynamic mobility is remarkably larger when Na^+ is selected as counterion, in comparison to the H^+ case, whatever the finite-size formalism chosen, although it is always larger with the C-S one. Likewise, there is also a clear shift of the mobility peak to larger frequencies for the H^+ counterions, due primarily to their larger diffusion coefficient (smaller drag coefficient). Note, however, that no finite counterion-size effects are necessary for such shift to take place, as it is also observed for the PL case [40,41]. In addition, and for each ionic species, it is observed another (smaller) frequency shift of the mobility peaks to larger frequencies when finite-size effects are allowed for. This can be related to the relaxation frequency shift already pointed out concerning the imaginary part of the complex relative permittivity for the Na^+ counterion case in Fig. 9(b). The same arguments can be extended to the H^+ case. Once more, the consideration of finite-size effects leads to very important changes in the predicted mobility in comparison with the standard pointlike predictions. The imaginary part of the mobility displayed in Fig. 10(b) confirms these arguments: The larger factor $n^{\text{max}} \delta$ for the C-S approach explains the relaxation frequency differences between PL and finite-size models [see also the analysis concerning the MW relaxation processes in Fig. 9(b)]. As regards the dielectric response

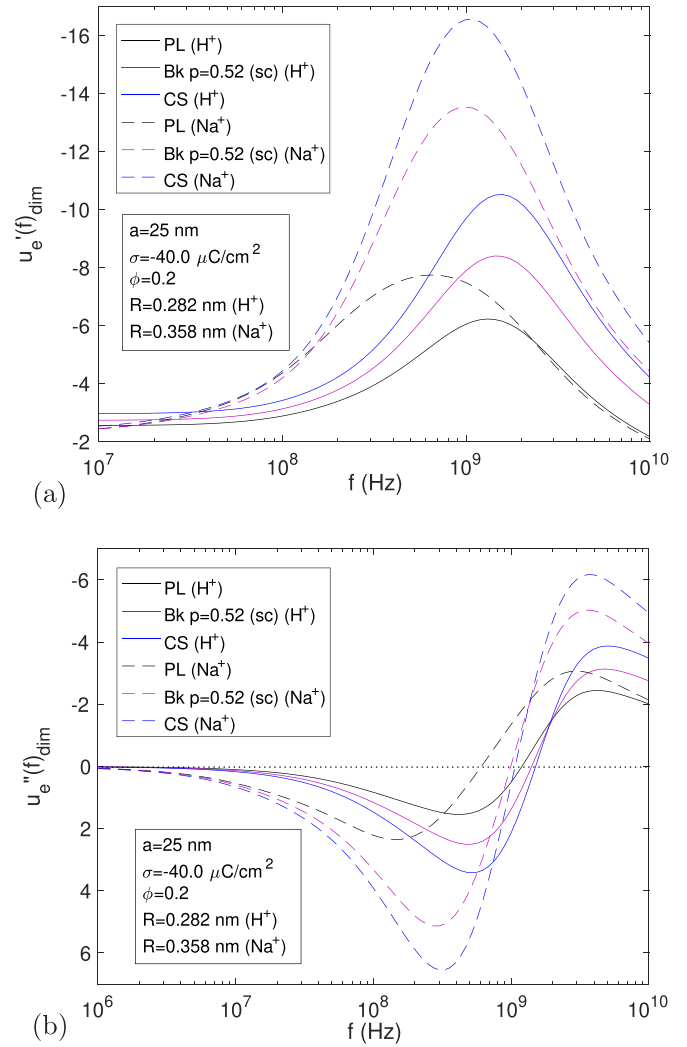


FIG. 10. (a) Dimensionless real part and (b) dimensionless imaginary part of the dynamic electrophoretic mobility as a function of frequency for salt-free colloids according to the PL, Bk [$p = 0.523$ (simple cubic packing)], and C-S approaches with different counterions: $R = 0.282$ nm (H^+) and $R = 0.358$ nm (Na^+), $a = 25$ nm, $\sigma = -40.0$ $\mu\text{C}/\text{cm}^2$, and $\phi = 0.2$.

of the salt-free colloid for Na^+ and H^+ , the real part of the relative permittivity as a function of frequency is compared in Fig. 11(a) for these two counterions following the PL, Bk, and C-S approaches. An increase in the low frequency response is observed for the Na^+ case over that for the H^+ one, a consequence of the larger polarizable structures in Na^+ , already mentioned. Also, a clear frequency shift of the global MW relaxation response to larger frequencies is found for the H^+ case due to its above mentioned larger diffusion coefficient.

These results are confirmed by the behavior of the imaginary component of the relative permittivity, displayed in Fig. 11(b). Here the frequencies of the MW relaxation processes are more clearly distinguished, specifically the change of the frequency of the global relaxation peak to larger values for the H^+ case [40,41]. A remarkable finding is that the relaxation frequency in presence of Na^+ is higher when finite-size ions are considered. In contrast, in line with our analysis of

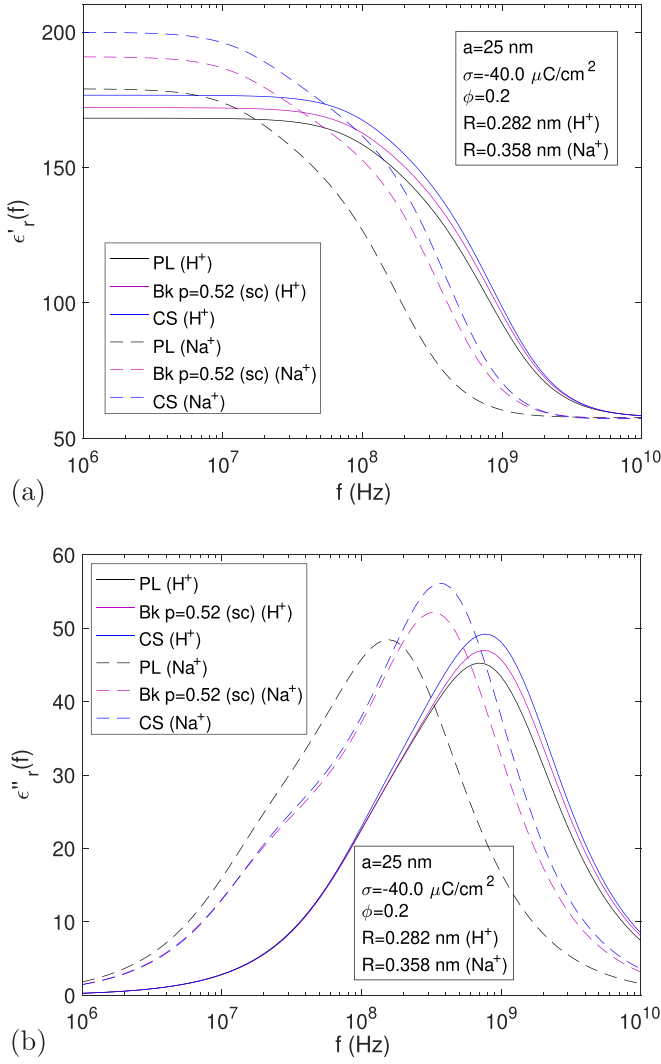


FIG. 11. (a) Real part and (b) imaginary part of the complex relative permittivity as a function of frequency for salt-free colloids according to the PL, Bk [$p = 0.523$ (simple cubic packing)], and C-S approaches with different counterions: $R = 0.282$ nm (H^+) and $R = 0.358$ nm (Na^+), $a = 25$ nm, $\sigma = -40.0$ $\mu C/cm^2$, and $\phi = 0.2$.

Fig. 9(b), it can be concluded that the product $n^{\max}\delta$ seems to be nearly constant for the H^+ counterion species, whatever the finite-size approach chosen [Fig. 11(b)]. In fact, as shown in Fig. 3, the profile of H^+ concentration is closer to the pointlike predictions, because of the small size of this ion.

VII. CONCLUSIONS

Salt-free colloids have gained increasing interest for both experimentalists and theoreticians [6,7,38]. One of its main characteristics is that for highly charged colloids a layer of counterions condenses onto the surface of the particles, a phenomenon that has an important influence in the behavior of these systems [8,13]. As in ordinary colloids, when the concentration of ions in solution is high (i.e., the surface charge of the particles and/or their concentration is large) the simplest model of pointlike ions must be substituted by approaches considering that the volume of ions is finite. In the

present work, the objective is the analysis of the electrokinetic behavior in ac fields of salt-free colloidal systems in conditions where ion-size effects are expected to be important. Two models are used, namely the C-S and Bikerman ones (the latter for different packing options) [2–4]. The results have shown that counterion finite-size effects cannot be neglected for a rigorous calculation of most of the electrokinetic and dielectric properties in highly charged and concentrated colloids. Thus, the electrophoretic mobility and the electrical conductivity increase very remarkably when finite ions are considered. The less effective screening of the particle charge in this case may help in explaining this behavior. Also, the changes in the counterion fluxes around the particles as the ions are expelled to farther regions from the particle surface because of their excluded volume, are decisive for understanding the observed responses [36]. These features are confirmed by explicit calculations based on the assumption of two widely different counterions, H^+ and Na^+ . Results on ac electrokinetics are particularized for dynamic mobility and dielectric dispersion spectra. In the former case, we observe a maximum in its real part, associated to the relaxation of two Maxwell-Wagner processes related to the diffuse (MWO) and condensed (MWC) layers, followed by a final decrease because of the inertia at the highest frequencies explored. The consideration of finite size of the ions leads to a shift to larger frequencies of the MWC relaxation frequency. This is justified by the dependence of that frequency on the product $n_{\max} \cdot \delta$, with n_{\max} the maximum counterion concentration allowed by size and δ the thickness of the condensate [36]. The results are confirmed by dielectric dispersion, where the MW relaxations are well observable and better separated than in dynamic mobility data. As a final conclusion, the finite ion size effect will surely have important effects on the electrokinetic properties of colloids for many applications with nanofluidic devices [48]. For such situations, it has been reported that local changes in the counterion diffusion coefficient, solution permittivity and solution viscosity near highly charged interfaces, will give rise to important changes in the electrokinetic and dielectric response of the colloid [49]. These aspects will be addressed in a future work.

ACKNOWLEDGMENTS

Financial support from the Spanish Institutions: Ministerio de Ciencia, Innovación y Universidades (GC2018-098770-B-I00) and Junta de Andalucía and European Funds for Regional Development (BF-FQM-141-UGR18, PI20-00233, and P18-FR-3583) is gratefully acknowledged.

APPENDIX: SOLUTION OF THE EQUILIBRIUM MODIFIED POISSON-BOLTZMANN EQUATION

By differentiating Eq. (9) we obtain:

$$\frac{dn^0(r)}{dr} = -\frac{ze}{k_B T} n^0(r) \frac{d\Psi^0(r)}{dr} - n^0(r) \frac{d \ln \gamma^0(r)}{dr} \quad (A1)$$

and similarly for the natural logarithm of $\gamma^0(r)$ in Eq. (1) or Eq. (3), we obtain:

$$n^0(r) \frac{d \ln \gamma^0(r)}{dr} = \Upsilon(r) \frac{dn^0(r)}{dr}, \quad (A2)$$

the $\Upsilon(r)$ function for the C-S case being defined as:

$$\Upsilon(r)_{\text{CS}} = \frac{8\varphi^0(r) - 2\varphi^0(r)^2}{[1 - \varphi^0(r)]^4} \quad (\text{A3})$$

and for the Bikerman case as:

$$\Upsilon(r)_{\text{Bk}} = \frac{\left[\frac{n^0(r)}{n^{\text{max}}}\right]}{1 - \left[\frac{n^0(r)}{n^{\text{max}}}\right]} = \frac{\varphi^0(r)}{p\left[1 - \frac{\varphi^0(r)}{p}\right]}. \quad (\text{A4})$$

By substituting the latter equations in the right part of Eq. (A1) we get:

$$\frac{dn^0(r)}{dr}[1 + \Upsilon(r)] = -\frac{ze}{k_B T} n^0(r) \frac{d\Psi^0(r)}{dr} \quad (\text{A5})$$

and with the help of Eq. (22) and its first radial derivative:

$$\frac{dn^0(r)}{dr} = -\frac{\varepsilon_0 \varepsilon_{\text{rs}}}{ze} \left[\frac{d^3\Psi^0(r)}{dr^3} + \frac{2}{r} \frac{d^2\Psi^0(r)}{dr^2} - \frac{2}{r^2} \frac{d\Psi^0(r)}{dr} \right], \quad (\text{A6})$$

Eq. (A5) becomes

$$\begin{aligned} & \frac{d^3\Psi^0(r)}{dr^3} + \frac{2}{r} \frac{d^2\Psi^0(r)}{dr^2} - \frac{2}{r^2} \frac{d\Psi^0(r)}{dr} \\ &= -\frac{ze}{k_B T} \left[\frac{d^2\Psi^0(r)}{dr^2} + \frac{2}{r} \frac{d\Psi^0(r)}{dr} \right] \frac{d\Psi^0(r)}{dr} \Lambda(r) \end{aligned} \quad (\text{A7})$$

and the $\Lambda(r)$ function for the C-S and Bk cases are given by:

$$\begin{aligned} \Lambda(r)_{\text{CS}} &= \frac{1}{1 + \Upsilon(r)_{\text{CS}}} \\ &= \frac{1 - 4\varphi^0(r) + 6\varphi^0(r)^2 - 4\varphi^0(r)^3 + \varphi^0(r)^4}{1 + 4\varphi^0(r) + 4\varphi^0(r)^2 - 4\varphi^0(r)^3 + \varphi^0(r)^4}, \end{aligned} \quad (\text{A8})$$

$$\begin{aligned} \Lambda(r)_{\text{Bk}} &= \frac{1}{1 + \Upsilon(r)_{\text{Bk}}} \\ &= 1 - \left[\frac{n^0(r)}{n^{\text{max}}} \right] = 1 - \left[\frac{\varphi^0(r)}{p} \right] = \frac{1}{\gamma_{\text{Bk}}^0(r)}. \end{aligned} \quad (\text{A9})$$

According to Eqs. (2) and (22), the counterion volume fraction can be expressed as a function of the equilibrium electrical potential as:

$$\varphi^0(r) = -\frac{\varepsilon_0 \varepsilon_{\text{rs}}}{ze} V_c \left[\frac{d^2\Psi^0(r)}{dr^2} + \frac{2}{r} \frac{d\Psi^0(r)}{dr} \right]. \quad (\text{A10})$$

The nonlinear third-order differential equation expressed by Eq. (A7) with the additional Eqs. (A8)–(A10) and the three boundary conditions shown in Eqs. (16) and (17) can be numerically solved in a single step to give the equilibrium electric potential $\Psi^0(r)$. Then, the equilibrium counterion concentration $n^0(r)$ can be derived by using Eq. (22). Its value on the outer surface of the cell $n^0(b)$, displayed in Eq. (10), is immediately obtained by particularizing Eq. (22) at $r = b$:

$$n^0(b) = -\frac{\varepsilon_0 \varepsilon_{\text{rs}}}{ze} \frac{d^2\Psi^0(r)}{dr^2} \Big|_{r=b}. \quad (\text{A11})$$

The pointlike case is easily recovered by making $\varphi^0(r) \rightarrow 0$ in Eqs. (A8) and (A9), yielding $\Lambda(r) \rightarrow 1$ and leading Eq. (A7) to become

$$\begin{aligned} & \frac{d^3\Psi^0(r)}{dr^3} + \frac{2}{r} \frac{d^2\Psi^0(r)}{dr^2} - \frac{2}{r^2} \frac{d\Psi^0(r)}{dr} \\ &= -\frac{ze}{k_B T} \left[\frac{d^2\Psi^0(r)}{dr^2} + \frac{2}{r} \frac{d\Psi^0(r)}{dr} \right] \frac{d\Psi^0(r)}{dr}. \end{aligned} \quad (\text{A12})$$

a result that was already derived in a previous paper [36] for an ideal salt-free colloid with pointlike released counterions. The derivation of the $\Lambda(r)$ function has allowed us to generalize in a simple way the Poisson-Boltzmann equation for the equilibrium electrical potential in salt-free colloids with pointlike counterions [compare Eq. (A7) and Eq. (A12)] to account for their finite size. Also, the way this $\Lambda(r)$ function has been defined has helped us to easily generalize the set of electrokinetic equations for salt-free colloids in constant or alternating electric fields, as it encompasses the effects of the counterion finite size. These studies have been addressed in this work.

-
- [1] F. Carrique, E. Ruiz-Reina, F. J. Arroyo, and Á. V. Delgado, Influence of ion size effects on the electrokinetics of aqueous salt-free colloids in alternating electric fields, *Phys. Rev. E* **102**, 032614 (2020).
- [2] J. Bikerman, XXXIX. Structure and capacity of electrical double layer, *Philos. Mag.* **33**, 384 (1942).
- [3] J. López-García, J. Horno, and C. Grosse, Ion size effects on the dielectric and electrokinetic properties in aqueous colloidal suspensions, *Curr. Opin. Colloid Interface Sci.* **24**, 23 (2016).
- [4] N. F. Carnahan and K. E. Starling, Equation of state for nonattracting rigid spheres, *J. Chem. Phys.* **51**, 635 (1969).
- [5] H. Ohshima, Electrokinetic phenomena in a dilute suspension of spherical colloidal particles in a salt-free medium, *Colloids Surf. A* **222**, 207 (2003).
- [6] F. Carrique, E. Ruiz-Reina, F. J. Arroyo, and Á. V. Delgado, Cell model of the direct current electrokinetics in salt-free concentrated suspensions: The role of boundary conditions, *J. Phys. Chem. B* **110**, 18313 (2006).
- [7] H. Ohshima, Ion size effect on counterion condensation around a spherical colloidal particle in a salt-free medium containing only counterions, *Colloid Polym. Sci.* **296**, 1293 (2018).
- [8] D. A. J. Gillespie, J. E. Hallett, O. Elujoba, A. F. Che Hamzah, R. M. Richardson, and P. Bartlett, Counterion condensation on spheres in the salt-free limit, *Soft Matter* **10**, 566 (2014).
- [9] Á. V. Delgado, F. Carrique, R. Roa, and E. Ruiz-Reina, Recent developments in electrokinetics of salt-free concentrated suspensions, *Curr. Opin. Colloid Interface Sci.* **24**, 32 (2016).
- [10] T. Y. Wang, H. T. Li, Y. J. Sheng, and H. K. Tsao, Equilibrium sedimentation profile of dilute, salt-free charged colloids, *J. Chem. Phys.* **129**, 204504 (2008).
- [11] T. Y. Wang, Y. J. Sheng, and H. K. Tsao, Donnan potential of dilute colloidal dispersions: Monte Carlo simulations, *J. Colloid Interface Sci.* **340**, 192 (2009).
- [12] T. Palberg, Crystallization kinetics of colloidal model suspensions: Recent achievements and new perspectives, *J. Phys.: Condens. Matter* **26**, 333101 (2014).

- [13] G. S. Manning, Counterion condensation on charged spheres, cylinders, and planes, *J. Phys. Chem. B* **111**, 8554 (2007).
- [14] G. Tellez, Nonlinear screening of charged macromolecules, *Philos. Trans. R. Soc. A* **369**, 322 (2011).
- [15] G. S. Manning, A counterion condensation theory for the relaxation, rise, and frequency dependence of the parallel polarization of rodlike polyelectrolytes, *Eur. Phys. J. E* **34**, 39 (2011).
- [16] I. Adroher-Benítez, S. Ahualli, D. Bastos-González, J. Ramos, J. Forcada, and A. Moncho-Jordá, The effect of electrosteric interactions on the effective charge of thermoresponsive ionic microgels: Theory and experiments, *J. Polym. Sci. Part B: Polym. Phys.* **54**, 2038 (2016).
- [17] M. Dubois, B. Deme, T. Gulik-Krzywicki, J.-C. Dedieu, C. Vautrin, S. Désert, E. Perez, and T. Zemb, Self-assembly of regular hollow icosahedra in salt-free catanionic solutions, *Nature (Lond.)* **411**, 672 (2001).
- [18] H. Zhang, J. Sun, X. Xin, W. Xu, J. Shen, Z. Song, and S. Yuan, Modulating self-assembly behavior of a salt-free peptide amphiphile (pa) and zwitterionic surfactant mixed system, *J. Colloid Interface Sci.* **467**, 43 (2016).
- [19] A. Chatterji and J. Horbach, The role of effective charges in the electrophoresis of highly charged colloids, *J. Phys.: Condens. Matter* **22**, 494102 (2010).
- [20] G. N. Smith, P. Brown, C. James, R. Kemp, A. M. Khan, T. S. Plivelic, S. E. Rogers, and J. Eastoe, The effects of counterion exchange on charge stabilization for anionic surfactants in nonpolar solvents, *J. Colloid Interface Sci.* **465**, 316 (2016).
- [21] G. N. Smith, L. L. Mears, S. E. Rogers, and S. P. Armes, Synthesis and electrokinetics of cationic spherical nanoparticles in salt-free non-polar media, *Chem. Sci.* **9**, 922 (2018).
- [22] B. E. Valley, A. D. Crowell, J. E. Butler, and A. J. Ladd, Electro-hydrodynamic extraction of dna from mixtures of dna and bovine serum albumin, *Analyst* **145**, 5532 (2020).
- [23] X. Vecino, G. Bustos, R. Devesa-Rey, J. Cruz, and A. Moldes, Salt-free aqueous extraction of a cell-bound biosurfactant: A kinetic study, *J. Surfactants Deterg.* **18**, 267 (2015).
- [24] V. Plakunov and M. Kokoeva, Osmostabilization of the cells of halobacteria and preparation of their dry biomass free of salts, *Microbiology* **63**, 338 (1994).
- [25] L. Wang, W. Ma, S. Zhang, X. Teng, and J. Yang, Preparation of cationic cotton with two-bath pad-bake process and its application in salt-free dyeing, *Carbohydr. Polym.* **78**, 602 (2009).
- [26] P. Tang, L. M. E. Lockett, M. Zhang, and G. Sun, Modification of cotton fabrics with 2-diethylaminoethyl chloride for salt-free dyeing with anionic dyes, *Cellulose* **28**, 6699 (2021).
- [27] J. J. López-García, J. Horno, and C. Grosse, Numerical solution of the electrokinetic equations for multi-ionic electrolytes including different ionic size related effects, *Micromachines* **9**, 647 (2018).
- [28] E. Mádai, B. Matejczyk, A. Dallos, M. Valiskó, and D. Boda, Controlling ion transport through nanopores: Modeling transistor behavior, *Phys. Chem. Chem. Phys.* **20**, 24156 (2018).
- [29] P. P. Gopmandal, S. De, S. Bhattacharyya, and H. Ohshima, Impact of ion-steric and ion-partitioning effects on electrophoresis of soft particles, *Phys. Rev. E* **102**, 032601 (2020).
- [30] P. Mahapatra, H. Ohshima, and P. P. Gopmandal, Electrophoresis of liquid-layer coated particles: Impact of ion partitioning and ion steric effects, *Langmuir* **37**, 11316 (2021).
- [31] J. J. López-García, J. Horno, and C. Grosse, Transport properties in nanochannels: Ionic size-, permittivity-, and viscosity-related effects, *J. Phys. Chem. C* **124**, 10764 (2020).
- [32] S. Kuwabara, The forces experienced by randomly distributed parallel circular cylinders or spheres in a viscous flow at small reynolds numbers, *J. Phys. Soc. Jpn.* **14**, 527 (1959).
- [33] E. K. Zholkovskij, J. H. Maslyiah, V. N. Shilov, and S. Bhattachaljee, Electrokinetic phenomena in concentrated disperse systems: General problem formulation and spherical cell approach, *Adv. Colloid Interface Sci.* **134-135**, 279 (2007).
- [34] J. J. López-García, J. Horno, and C. Grosse, Differential capacitance of the diffuse double layer at electrode-electrolyte interfaces considering ions as dielectric spheres: Part I. Binary electrolyte solutions, *J. Colloid Interface Sci.* **496**, 531 (2017).
- [35] E. Ruiz-Reina and F. Carrique, Electric double layer of spherical particles in salt-free concentrated suspensions: Water dissociation and CO₂ influence, *J. Phys. Chem. B* **112**, 11960 (2008).
- [36] R. Roa, F. Carrique, and E. Ruiz-Reina, dc electrokinetics for spherical particles in salt-free concentrated suspensions including ion size effects, *Phys. Chem. Chem. Phys.* **13**, 19437 (2011).
- [37] C. Zhong, Y. Deng, W. Hu, J. Qiao, L. Zhang, and J. Zhang, A review of electrolyte materials and compositions for electrochemical supercapacitors, *Chem. Soc. Rev.* **44**, 7484 (2015).
- [38] H. Ohshima, Dynamic electrophoretic mobility of spherical colloidal particles in a salt-free medium, *J. Colloid Interface Sci.* **265**, 422 (2003).
- [39] F. Carrique, E. Ruiz-Reina, F. J. Arroyo, M. Jiménez, and Á. V. Delgado, Dielectric response of a concentrated colloidal suspension in a salt-free medium, *Langmuir* **24**, 11544 (2008).
- [40] R. Roa, F. Carrique, and E. Ruiz-Reina, Ion size effects on the electrokinetics of salt-free concentrated suspensions in ac fields, *J. Colloid Interface Sci.* **387**, 153 (2012).
- [41] F. Carrique, E. Ruiz-Reina, R. Roa, F. J. Arroyo, and Á. V. Delgado, Ionic coupling effects in dynamic electrophoresis and electric permittivity of aqueous concentrated suspensions, *Colloids Surf. A* **541**, 195 (2018).
- [42] R. O'Brien, D. Cannon, and W. Rowlands, Electroacoustic determination of particle size and zeta potential, *J. Colloid Interface Sci.* **173**, 406 (1995).
- [43] H. Ohshima, Dynamic electrophoretic mobility of spherical colloidal particles in concentrated suspensions, *J. Colloid Interface Sci.* **195**, 137 (1997).
- [44] J. R. Guzman-Sepulveda, S. Amin, E. N. Lewis, and A. Dogariu, Full characterization of colloidal dynamics at low Péclet numbers, *Langmuir* **31**, 10351 (2015).
- [45] F. Carrique, E. Ruiz-Reina, F. J. Arroyo, M. L. Jiménez, and Á. V. Delgado, Dynamic electrophoretic mobility of spherical

- colloidal particles in salt-free concentrated suspensions, *Langmuir* **24**, 2395 (2008).
- [46] H. Ohshima, Electrophoretic mobility of a spherical colloidal particle in a salt-free medium, *J. Colloid Interface Sci.* **248**, 499 (2002).
- [47] M. Aranda-Rascón, C. Grosse, J. López-García, and J. Horno, Electrokinetics of suspended charged particles taking into account the excluded volume effect, *J. Colloid Interface Sci.* **335**, 250 (2009).
- [48] J. Hoffmann and D. Gillespie, Ion correlations in nanofluidic channels: Effects of ion size, valence, and concentration on voltage- and pressure-driven currents, *Langmuir* **29**, 1303 (2013).
- [49] J. J. López-García, J. Horno, and C. Grosse, Ionic size, permittivity, and viscosity-related effects on the electrophoretic mobility: A modified electrokinetic model, *Phys. Rev. Fluids* **4**, 103702 (2019).